

Article

Dynamic Harris Hawks Optimization with Mutation Mechanism for Satellite Image Segmentation

Heming Jia ¹ , Chunbo Lang ¹ , Diego Oliva ² , Wenlong Song ^{1,*} and Xiaoxu Peng ¹ 

¹ College of Mechanical and Electrical Engineering, Northeast Forestry University, Harbin 150040, China; jiaheming@nefu.edu.cn (H.J.); langchunbo@nefu.edu.cn (C.L.); pengxiaoxu@nefu.edu.cn (X.P.)

² Depto. de Ciencias Computacionales, Universidad de Guadalajara, CUCEI, Av. Revolución 1500, Guadalajara C.P. 44100, Jalisco, Mexico; diego.oliva@cucei.udg.mx

* Correspondence: swl@nefu.edu.cn

Received: 2 May 2019; Accepted: 12 June 2019; Published: 14 June 2019



Abstract: In this paper, a novel satellite image segmentation technique based on dynamic Harris hawks optimization with a mutation mechanism (DHHO/M) is proposed. Compared with the original Harris hawks optimization (HHO), the dynamic control parameter strategy and mutation operator used in DHHO/M can avoid falling into the local optimum and efficiently enhance the search capability. To evaluate the performance of the proposed method, a series of experiments are carried out on various satellite images. Eight advanced thresholding approaches are selected for comparison. Three criteria are adopted to determine the segmentation thresholds, namely Kapur's entropy, Tsallis entropy, and Otsu between-class variance. Furthermore, four oil pollution images are used to further assess the practicality and feasibility of the proposed method on real engineering problem. The experimental results illustrate that the DHHO/M based thresholding technique is superior to others in the following three aspects: fitness function evaluation, image segmentation effect, and statistical tests.

Keywords: satellite image; thresholding; image segmentation; Harris hawks optimization; mutation mechanism; Kapur's entropy

1. Introduction

Image segmentation is a fundamental and crucial stage in some applications, such as computer vision, pattern recognition, image classification, etc. [1–4]. Generally speaking, the purpose of the segmentation operation is to partition the grayscale or color image into several non-overlapping regions with unique characteristics. The gray levels of the pixels in the same area are roughly the same, while the pixels from different areas are significantly different. In the last few decades, many segmentation methods have been proposed by scholars, such as clustering, fractal-wavelet modeling, region growing, and thresholding [5–7]. Among all available techniques, threshold-based (thresholding) method is extensively used due its simplicity and efficiency [8,9].

Thresholding technique can be mainly divided into two categories: bi-level and multilevel [10]. Bi-level thresholding splits the image into two classes according to the intensity. However, if the image contains much information and multiple objects, the bi-level thresholding is not competent. Therefore, as an extension of bi-level thresholding, multilevel thresholding is proposed to handle the current issues [11]. For example, Díaz–Cortés et al. segment the breast thermograms using multilevel thresholding, which provides a highly reliable clinical decision support and advances the progress of thresholding approach in medical imaging domain [12]. Also, multilevel thresholding is adopted by Bhandari et al. to process the satellite images, which improves the segmentation accuracy and obtains high-quality segmented images [13]. In fact, researchers have introduced numerous approaches

based on different criteria to select the segmentation thresholds over the past few decades, such as Kapur's entropy [14], Tsallis entropy [15], and Otsu between-class variance [16]. Kapur's entropy measures the homogeneity of segmented regions by maximizing the histogram entropy. Tsallis entropy also determines the thresholds by maximizing the entropy, but there are certain constraints. Otsu's technique maximizes the between-class variance of the segmented image.

Multilevel thresholding can be considered as a NP-hard problem with high complexity [10]. To be more specific, the computational complexity increases exponentially with the number of thresholds, which greatly affects the efficiency and feasibility. To overcome this drawback, meta-heuristic algorithms are introduced into this domain and combined with the thresholding technique. In 2017, He and Huang proposed a modified firefly algorithm (MFA) based method to select the segmentation thresholds [11]. Kapur's entropy, Otsu between-class variance, and minimum cross entropy are served as fitness functions. Experimental results reveal that the proposed technique can efficiently reduce the computational complexity and produce segmented images with more details. Khairuzzaman and Chaudhury combined the grey wolf optimizer (GWO) with thresholding for grayscale image segmentation [7]. Kapur's entropy and Otsu's method are used to select the segmentation thresholds. It can be found from the results that the proposed approach can accurately determine the segmentation thresholds and significantly reduce the computational complexity. In 2017, Oliva et al. presented an efficient magnetic resonance (MR) image segmentation method based on crow search algorithm (CSA) and minimum cross entropy [17]. The results of the comparison experiment show that the well-delimited regions obtained are easier to distinguish than other techniques [17]. Furthermore, some other algorithms or their modified versions have also been introduced into this domain, such as whale optimization algorithm (WOA) [18], multi-verse optimizer (MVO) [19], grasshopper optimization algorithm (GOA) [20], social spiders optimization (SSO) [21], krill herd optimization (KHO) [22], and cuckoo search (CS) [23] as well as Lévy flight firefly algorithm (LFA) [24], hybrid differential evolution (hjDE) [25], adaptive wind driven optimization (AWDO) [26], etc. These promising results motivate us to apply some other efficient meta-heuristic algorithms to multilevel image thresholding. Besides, as stated in No-Free Lunch Theorem (NFL) [27], there is no algorithm can solve all optimization problems. Thus, the recently proposed and uninvestigated algorithm also has potential.

Harris hawks optimization (HHO) is a high-performance, population-based, gradient-free optimization technique, which was proposed by Heidari et al. in 2019 [28]. Inspired from the cooperative behavior and chasing style of Harris hawks in nature, the mathematical model of HHO was established [28]. Similar to other meta-heuristic algorithms, the exploration and exploitation stages are also included in HHO. Each Harris hawk represents a candidate solution in the search space and the best solution obtained so far is considered as the prey or approximate optimal solution. During the whole process of predation, the Harris hawks patiently wait for the prey, besiege the prey to make it exhausted, and finally attack the prey with a surprise pounce. According to [28], HHO has presented better or occasionally competitive results than well-established techniques on 29 benchmark problems and several real-world engineering tasks. These phenomena illustrate the potential and the superiority of HHO, which also motivates us to apply this powerful algorithm to multilevel image thresholding.

No algorithm is perfect. Each algorithm requires some adjustments to fit the current problem, as does the HHO algorithm. For example, the exploration and exploitation phases of HHO are unbalanced. To be more specific, the absolute value of the parameter E cannot be larger than 1 during the latter half of the iteration (e.g., the last 250 of 500 maximum iterations), that is, the search agent does not perform a global search, although the current region may not be promising. For some complex optimization tasks, there is no guarantee that the population has gathered near the global optimum at the end of the exploration phase, resulting in premature convergence and local optimization. Therefore, two improvement strategies are introduced in this paper to enhance the optimization ability of the original HHO. As for the former, a novel dynamic control parameter strategy is presented to avoid trapping into the local optimum. The essence of the improvement strategy is to add a disturbance term to the update formulation of the escaping energy (E). Sine and cosine functions are used in combination

to control where the disturbance peak appears. A Gaussian distribution is also adopted to increase randomness. In the experiment, not only the influence of parameter change on the performance of disturbance term, but also the reason for using the Gaussian distribution instead of the Levy distribution is analyzed. As for the latter, a famous mutation operator, known as DE/best/2 is utilized to improve the global search efficiency and population diversity [29]. Then, the modified version of HHO, known as dynamic Harris hawks optimization with a mutation mechanism (DHHO/M) is applied to multilevel image thresholding.

Satellite imagery contains a wealth of information and is crucial to environmental resource monitoring and evaluation, such as forest cover, wetland resources, climate change, etc. Although remote sensing technology has many advantages (e.g., fast update cycle, fewer interference factors, and saving manpower and material resources), it is still a challenge to extract boundaries, locate objects and separate regions in high-resolution satellite images [30]. To solve the above problems, DHHO/M is combined with thresholding technique for satellite image segmentation. A series of experiment are carried out to evaluate the performance of the proposed method. The experiments can be mainly divided into four parts. For the first part, the impact of both the improvement strategies on performance is investigated and analyzed. For the second and the most important part, the DHHO/M based approach is compared with four advanced thresholding techniques on satellite images. Various performance metrics have been taken into consideration, such as objective function value, standard deviation (Std), peak signal to noise ratio (PSNR), mean squared error (MSE), structural similarity index (SSIM), feature similarity index (FSIM), and convergence property as well as the Wilcoxon's rank sum test and Friedman test. For the third part, DHHO/M is compared with other thresholding techniques based on different criteria. For the fourth part, four oil pollution images are used to further assess its practicality and feasibility on real engineering problems.

The contributions of this paper have three aspects:

1. Introduce the recently proposed HHO into multilevel image thresholding. To the best of the authors' knowledge, this attempt has not been made yet.
2. Dynamic control parameter strategy and mutation mechanism are used to improve the search efficiency of the original HHO.
3. Objectively and comprehensively evaluate the performance of the proposed technique.

The structure of this paper is described as follows: in Section 2, the problem statement and definitions of Kapur's entropy, Tsallis entropy, and Otsu's method are given. Section 3 briefly reviews the original HHO. In Section 4, the proposed DHHO/M based image thresholding technique is introduced in details. Section 3 presents the experimental results and relevant discussions. Finally, the conclusion and future research direction are represented in the last section.

2. Material and Methods

2.1. Problem Statement

For multilevel image thresholding, the ultimate goal is to select the combination of segmentation thresholds. Assume that the given image is segmented into $n + 1$ classes $\{C_0, C_1, \dots, C_n\}$ by n thresholds $\{T_1, T_2, \dots, T_n\}$, which can be defined as follows [31]:

$$\begin{aligned} C_0 &= \{I(i, j) | 0 \leq I(i, j) \leq T_1 - 1\} \\ C_1 &= \{I(i, j) | T_1 \leq I(i, j) \leq T_2 - 1\} \\ &\dots \\ C_k &= \{I(i, j) | T_k \leq I(i, j) \leq L - 1\} \end{aligned} \quad (1)$$

where $I(i, j)$ denotes the gray level of the (i, j) th pixel, and L is the number of gray levels in the given image.

Furthermore, the combination of the optimal thresholds is determined by optimizing (maximizing or minimizing) the objective function, which is mathematically expressed as the following equations:

$$\{T_1^*, T_2^*, \dots, T_n^*\} = \arg \max_{T_1, \dots, T_n} f(T_1, T_2, \dots, T_n), \tag{2}$$

$$\{T_1^*, T_2^*, \dots, T_n^*\} = \arg \min_{T_1, \dots, T_n} f(T_1, T_2, \dots, T_n), \tag{3}$$

where f represents the objective function and $\{T_1^*, T_2^*, \dots, T_n^*\}$ is the combination of the optimal thresholds.

2.2. Multilevel Thresholding

2.2.1. Kapur’s Entropy

Kapur’s entropy is a famous thresholding method that selects the thresholds based on the entropy of the segmented classes [14]. The objective function can be defined as:

$$f_{Kapur} = \sum_{i=0}^n H_i, H_i = - \sum_{j=T_i}^{T_{i+1}-1} \frac{p_j}{\omega_i} \ln\left(\frac{p_j}{\omega_i}\right), \tag{4}$$

where $\omega_i = \sum_{j=T_i}^{T_{i+1}-1} p_j$, $p_j = h(j)/N$. ω_i indicates the sum of the probabilities of the pixels in the i th class, p_j is the proportion of pixels in each gray level to the total, $h(j)$ represents the frequency, and N is the number of all pixels. Besides, for multilevel image thresholding, $T_0 = 0$ and $T_{n+1} = L$.

2.2.2. Tsallis Entropy

Tsallis entropy is extensively used by researchers in the field of image thresholding to choose the optimal combination of thresholds [15]. The objective function is mathematically represented as:

$$f_{Tsallis} = \sum_{i=0}^n S_q^{ci} + (1 - q) \prod_{i=0}^n S_q^{ci}, S_q^{ci} = \frac{1 - \sum_{j=T_i}^{T_{i+1}-1} \left(\frac{p_j}{\omega_i}\right)^q}{q - 1}, \tag{5}$$

where q is a constant equal to 4, the value selected is the same as [30,32].

2.2.3. Otsu Between-Class Variance

Otsu’s method was proposed in 1979, which maximizes the between-class variance of segmented classes to determine the thresholds [16]. The objective function is presented as follows:

$$f_{Otsu} = \sum_{i=0}^n \sigma_i^2, \sigma_i^2 = \sum_{j=T_i}^{T_{i+1}-1} \omega_i (\mu_i - \bar{\mu}), \tag{6}$$

where $\mu_i = \sum_{j=T_i}^{T_{i+1}-1} \frac{jp_j}{\omega_i}$, $\bar{\mu} = \sum_{j=0}^{L-1} jp_j$. $\bar{\mu}$ is the mean intensity for whole image.

The mathematical form of above three optimization problems can be expressed as:

Consider $\vec{x} = [x_1, x_2, \dots, x_n]$.

Maximize $f_{Kapur}(\vec{x}) = - \sum_{i=0}^n \sum_{j=x_i}^{x_{i+1}-1} \frac{p_j}{\omega_i} \ln\left(\frac{p_j}{\omega_i}\right)$

or

$$f_{Tsallis}(\vec{x}) = \sum_{i=0}^n \frac{1 - \sum_{j=x_i}^{x_{i+1}-1} \left(\frac{p_j}{\omega_i}\right)^q}{q - 1} + (1 - q) \prod_{i=0}^n \frac{1 - \sum_{j=x_i}^{x_{i+1}-1} \left(\frac{p_j}{\omega_i}\right)^q}{q - 1}$$

or

$$f_{Otsu}(\vec{x}) = \sum_{i=0}^n \sum_{j=x_i}^{x_{i+1}-1} \omega_i (\mu_i - \bar{\mu}).$$

Subject to x_i must be integer, $i = 1, 2, \dots, n$ Variable range $0 \leq x_i \leq 255$.

As discussed above, the computational complexity of the thresholding techniques will increase exponentially with the number of thresholds. Thus, meta-heuristic algorithms are used to optimize the objective functions in Equations (4)–(6) to improve the efficiency.

2.3. Harris Hawks Optimization

HHO is a novel population-based, gradient-free optimization technique, which was proposed by Heidari et al. in 2019 [28]. HHO simulates the predation, surprise pounce, and attacking behaviors of Harris hawks in nature. Similar to other meta-heuristic algorithms, HHO also includes two optimization stages, namely exploration and exploitation (see Figure 1), which are described in the following subsections.

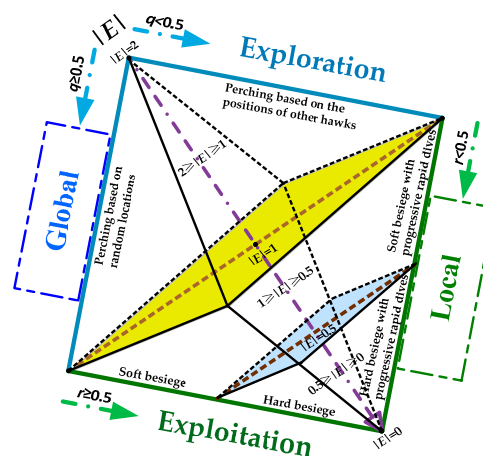


Figure 1. Different stages of Harris hawks optimization (HHO).

2.3.1. Exploration Stage

Harris hawks have insightful eyes that help them track and detect prey, however, sometimes the prey is not easy to find. Then, the Harris hawks will perch, wait patiently, and may last for hours. In HHO, above behaviors are modeled as the exploration stage, which can be expressed as:

$$X_i^{t+1} = \begin{cases} X_{rand}^t - r_1 |X_{rand}^t - 2r_2 X(t)| & q \geq 0.5 \\ (X_{rabbit} - X_m^t) - r_3 (LB + r_4 (UB - LB)) & q < 0.5' \end{cases} \quad (7)$$

where X_i^{t+1} is the position of i th individual in $(t + 1)$ th iteration, X_{rabbit} denotes the position of the rabbit (prey), and q is a random number in the interval $[0,1]$ that converts the two strategies. $r_1, r_2, r_3,$ and r_4 are also random numbers inside $[0,1]$. LB and UB are the upper and lower bounds of the given optimization problem respectively. X_m^t represents the average position of the population that can be calculated as follows:

$$X_m^t = \frac{1}{N} \sum_{i=1}^N X_i^t, \quad (8)$$

where N is the size of the population, and X_i^t is the position of i th individual in t th iteration.

2.3.2. Transition from Exploration to Exploitation

The transition between exploration and exploitation is critical to the performance of meta-heuristic algorithms. In HHO, the escaping energy of the rabbit, known as E , is used to convert these two phases. The value of E decreases as the number of iterations increases, which can be mathematically modelled as:

$$E = 2E_0 * \left(1 - \frac{t}{t_{max}}\right), \quad (9)$$

where E_0 is a random number that changes in the interval $[-1,1]$, t denotes the current iteration, and t_{\max} represents the maximum number of iterations.

More specifically, the value of E decreases from $[-2,2]$ to 0 as the iterative process. If $|E| \geq 1$, the exploration stage is used to search for the prey; If $|E| < 1$, the exploitation stage is adopted to exploit the promising area.

2.3.3. Exploitation Stage

After detecting the prey, the Harris hawks tend to attack it using surprise pounce. The actual predation process is often very complicated, the prey has a chance to escape and the Harris hawks also react differently according to the behavior of the prey. In order to better simulate the real situation, four strategies are used in the exploitation stage. A random number (r) is used to determine whether the prey has successfully escaped. The case $r < 0.5$ indicates successful escape, while $r \geq 0.5$ shows unsuccessful escape. The escaping energy of the prey (E) affects the behavior of the Harris hawks. If $|E| \geq 0.5$, the soft besiege occurs; if $|E| < 0.5$, the hard besiege happens [28].

A. Soft besiege

Considering $r \geq 0.5$ and $|E| \geq 0.5$, the rabbit has enough energy and keeps trying to escape, even though these acts are in vain and will only make the prey itself exhausted. At the same time, the Harris hawks softly encircle the rabbit and then attack it using surprise pounce. The mathematical model is given as follows:

$$X_i^{t+1} = \Delta X_i^t - E|JX_{\text{rabbit}} - X_i^t| \quad (10)$$

$$\Delta X_i^t = X_{\text{rabbit}} - X_i^t, \quad (11)$$

where ΔX_i^t indicates the difference between the position vector of the rabbit and the current individual. r_5 is a random number inside $[0,1]$, and $J = 2(1 - r_5)$ indicates the random jump strength of the rabbit during the escape process.

B. Hard besiege

Considering $r \geq 0.5$ and $|E| < 0.5$, the rabbit becomes so exhausted and does not have enough escaping energy. Meanwhile, the Harris hawks hardly encircle the rabbit to conduct the final pounce. This process can be modeled as:

$$X_i^{t+1} = X_{\text{rabbit}} - E|\Delta X_i^t|. \quad (12)$$

C. Soft besiege with progressive rapid dives

Considering $r < 0.5$ and $|E| \geq 0.5$, the rabbit has enough energy and managed to escape. In the meantime, a more intelligent soft besiege is performed before the surprise pounce. Note that the position update of the Harris hawks in this situation is a two-step process. If the first step is not an improved move, then the second step will be executed. For the former part, it can be mathematically modelled as:

$$Y = X_{\text{rabbit}} - E|JX_{\text{rabbit}} - X_i^t|. \quad (13)$$

For the latter part, the Levy flight is used to simulate the rapid, abrupt, and irregular movement of Harris hawks when chasing the rabbit. The formulation for position update is presented as:

$$Z = Y + S \times \text{Levy}(dim). \quad (14)$$

where dim is the dimensions of the optimization problem, S is a random vector of size $1 \times dim$, and Levy denotes the Levy distribution that is defined as:

$$\text{Levy}(x) = 0.01 \times \frac{u \times \sigma}{|v|^{\frac{1}{\beta}}}, \sigma = \left(\frac{\Gamma(1 + \beta) \times \sin\left(\frac{\pi\beta}{2}\right)^{\frac{1}{\beta}}}{\Gamma\left(\frac{1+\beta}{2}\right) \times \beta \times 2^{\left(\frac{\beta-1}{2}\right)}} \right)^{\frac{1}{\beta}}, \quad (15)$$

where u and v are random values in the interval $[0,1]$. β is a constant equal to 1.5.

Then, for a problem to be minimized, the mathematical model of the whole process at this stage is:

$$X_i^{t+1} = \begin{cases} Y & \text{if } f(Y) < f(X_i^t) \\ Z & \text{if } f(Z) < f(X_i^t) \end{cases} \quad (16)$$

where f is the fitness function for the given optimization problem.

D. Hard besiege with progressive rapid dives

Considering $r < 0.5$ and $|E| < 0.5$, the rabbit does not have enough energy but it successfully escapes. In this situation, the Harris hawks perform a hard besiege before the surprise pounce, and they try to bring the whole group closer to the prey, not just the individual. Therefore, the formulation for position update of the Harris hawks is given as follows:

$$X_i^{t+1} = \begin{cases} Y & \text{if } f(Y) < f(X_i^t) \\ Z & \text{if } f(Z) < f(X_i^t) \end{cases} \quad (17)$$

where

$$Y = X_{\text{rabbit}} - E|JX_{\text{rabbit}} - X_m^t| \quad (18)$$

$$Z = Y + S \times \text{Levy}(\text{dim}) \quad (19)$$

Furthermore, the pseudocode of HHO is represented in Algorithm 1.

Algorithm 1 Pseudocode of Harris hawks optimization (HHO) algorithm

Input: The size of population N , maximum number of iterations t_{max} .

Output: The position of the rabbit and the corresponding fitness function value.

1. Initialize the position of the hawks X_i and the rabbit X_{rabbit} .
 2. Initialize the fitness values of the hawks f_i and the rabbit f_{rabbit} .
 3. Set the dimensions of the optimization problem dim .
 4. **While** (termination condition is not met ($t < t_{\text{max}}$)) **do**
 5. Check the boundary and evaluate the fitness value of each hawk f_i .
 6. Update the location X_{rabbit} and fitness value f_{rabbit} of rabbit if there is a better one.
 7. **For** (each hawk ($i = 1 : N$)) **do**
 8. Update the energy of the rabbit E using Equation (9).
 9. **If** ($|E| \geq 1$) **then** % Exploration Stage
 10. Update the position using Equation (7).
 11. **Else If** ($|E| < 1$) **then** % Exploitation Stage
 12. **If** ($r \geq 0.5$ and $|E| \geq 0.5$) **then** % Soft besiege
 13. Update the position using Equation (10).
 14. **Else If** ($r \geq 0.5$ and $|E| < 0.5$) **then** % Hard besiege
 15. Update the position using Equation (12).
 16. **Else If** ($r < 0.5$ and $|E| \geq 0.5$) **then** % Soft besiege with progressive rapid dives
 17. Update the position using Equation (16).
 18. **Else If** ($r < 0.5$ and $|E| < 0.5$) **then** % Hard besiege with progressive rapid dives
 19. Update the position using Equation (17).
 20. **End If**
 21. **End If**
 22. **End For**
 23. **End While**
-

2.4. Proposed Dynamic Harris Hawks Optimization with Mutation Mechanism

In this section, the proposed DHHO/M algorithm based image segmentation technique is introduced in detail. For multilevel color image segmentation problem, the input to the method was the histogram of each color component, and the output was the segmentation thresholds. This process was implemented by optimizing the objective functions in Equations (4)–(6) using the DHHO/M algorithm. The following subsections will discuss the two improvement strategies respectively, and then give the algorithm steps. Finally, the time complexity of DHHO/M and HHO is analyzed.

2.4.1. Dynamic Control Parameter Strategy

In the original HHO algorithm, the transition of the exploration and exploitation phase is based on the escaping energy (E) of the rabbit. More specifically, the absolute value of the parameter E decreased from 2 to 0 throughout the whole iteration. If $|E| > 1$, HHO explored the search space to determine the promising area. On the contrary, if $|E| < 1$, the exploitation strategy was adopted to enhance the local search efficiency. However, the main drawback of this transition process is that the absolute value of the parameter E cannot be larger than 1 during the latter half of the iteration (e.g., the last 250 of 500 maximum iterations), that is, the search agents do not perform global search during the second half of the iteration, although the current region may not be promising. For some complex optimization tasks, there was no guarantee that the population has gathered near the global optimum at the end of the exploration phase, resulting in premature convergence and local optimal values.

Therefore, a novel dynamic control parameter strategy is introduced with the purpose of jumping out of the local optimum under the premise of ensuring accuracy. The essence of the improvement strategy is to add a disturbance term to the update formulation of E in Equation (9). The disturbance term and modified update formulation of E are presented as follows:

$$\delta = randn * \left(\sin^{\alpha} \left(\frac{\pi}{2} * \frac{t}{t_{\max}} \right) + \cos \left(\frac{\pi}{2} * \frac{t}{t_{\max}} \right) - 1 \right) \quad (20)$$

$$E = 2E_0 * \left(1 - \frac{t}{t_{\max}} \right) + \delta, \quad (21)$$

where \sin and \cos denote the sine and cosine functions respectively. $randn$ is a random number subject to Gaussian distribution. t and t_{\max} represent the current iteration and the maximum number of iterations respectively. α is a constant that determines where the disturbance peak appears.

Figure 2 illustrates the variation of the disturbance term δ under different values of parameter α . It can be found that the amplitude decreases as the value of the parameter α increases, and the high amplitude disturbance occurs earlier when $\alpha = 2$.

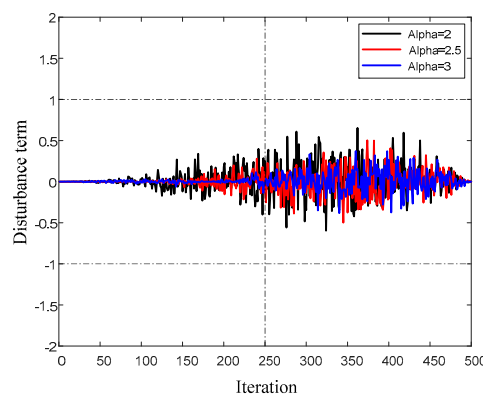


Figure 2. Variation of the disturbance term δ under different values of parameter α .

In order to more intuitively illustrate the impact of dynamic control parameter strategy on the escaping energy of the rabbit, the variation of the parameter E with the number of iterations is also

given in Figure 3. It is worth mentioning that the values of E was not only the key to global and local phases transition, but also affects the convergence of the algorithm because it was part of the position update formulation. To be more specific, a larger value indicates more exploration, while a smaller value indicates more exploitation. As can be observed from the figure, when $\alpha = 2$, the absolute value of E in the late iteration can be abruptly greater than 1, but the amplitude of the disturbance term is too large, which seriously affects the convergence performance. In the case of $\alpha = 3$, the amplitude of the perturbation term is too small, which cannot enhance the ability of jumping out of the local optimum, but will not affect the performance of the algorithm itself. Considering $\alpha = 2.5$, it can be found that the convergence property was not greatly affected, and the global search strategy also had an opportunity to be adopted in the later iteration. As far as the authors are concerned, for optimizing some fitness functions that contain local best, setting α to 3 may reduce the accuracy; setting α to 2 made the results obtained similar to the original algorithm; while setting α to 2.5 can improve the performance of the algorithm. These hypotheses will be verified in the experimental section.

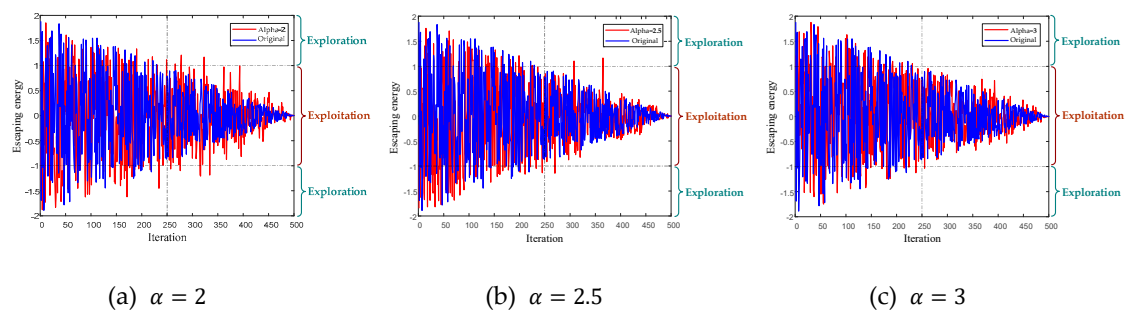


Figure 3. Variation of the escaping energy of the rabbit E under different values of parameter α .

In addition, it was necessary to explain the reason why the Gaussian distribution is used instead of the Levy distribution in the disturbance term. Although the characteristic of usually small steps and occasional large jumps in Levy distribution fits well with the idea of the improvement strategy, sometimes there are some extreme cases as shown in Figure 4, which can seriously affect the performance of the algorithm. More specifically, the disturbance of uncertain position makes the population evolve slowly and even degenerate.

Reducing the step size of Levy flight can theoretically improve this situation, but in fact, it is difficult to determine an appropriate value to meet the desired requirements. In our study, if the step size is larger than 0.05, disturbances with large amplitude will always appear; if the step size is smaller than 0.01, the disturbance is not enough to affect the value of E ; while the value between the two is still not ideal. Therefore, the Gaussian distribution is more suitable for the current problem, and the amplitude generated by it is acceptable compared with the Levy distribution.

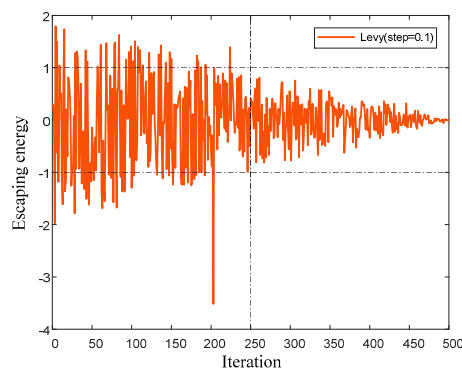


Figure 4. Variation of the escaping energy of the rabbit E using Levy distribution.

Furthermore, according to our experimental statistics, the disturbance peaks of our proposed strategy usually appeared during the 300th to 400th iterations (the maximum number of iterations was 500), especially the 350th to the 400th iterations.

2.4.2. Mutation Mechanism

In order to enhance the global search efficiency of HHO, mutation mechanism was introduced into the exploration stage. The famous DE/best/2 mutation operator was adopted to replace the original location update strategy in Equation (7) [29]. The formulation is given as follows:

$$X_i^{t+1} = X_{\text{best}}^t + F(X_{r_1}^t - X_{r_2}^t) + F(X_{r_3}^t - X_{r_4}^t), \quad (22)$$

where x_i^{t+1} indicates the position of the i th individual at the t th iteration, and F is the scaling factor. $r_1, r_2, r_3,$ and r_4 are different integers selected from the range $[1, N]$ and distinct from i . N denotes the size of population. Thus, Equation (7) can be rewritten as follows:

$$X_i^{t+1} = \begin{cases} X_{\text{best}}^t + F(X_{r_1}^t - X_{r_2}^t) + F(X_{r_3}^t - X_{r_4}^t) & q \geq 0.5 \\ (X_{\text{rabbit}}^t - X_m^t) - \text{rand}1 \times (LB + \text{rand}2 \times (UB - LB)) & q < 0.5' \end{cases} \quad (23)$$

where $\text{rand}1$ and $\text{rand}2$ are random numbers in the interval $[0,1]$.

The operators of differential evolution (DE) have been widely used as part of modified or hybrid algorithm to improve the optimization capability and search efficiency. This is also the motivation for us to adopt the mutation operator mentioned above. For example, Xiong et al. proposed a hybrid algorithm of whale optimization algorithm (WOA) and DE, known as DE/WOA, for extracting parameters of solar photovoltaic models [33]. DE/best/2 is utilized in this proposed algorithm with the purpose of improving the ability of exploring the search space and locating the region of global optimum [33]. Also, Jadon et al. used DE to modify the onlooker bee phase of artificial bee colony (ABC) algorithm [34]. DE/best/1 is adopted to accelerate the convergence speed and maintain population diversity. Furthermore, DE has also been embedded or merged into some other improved versions of meta-heuristic algorithm, such as moth search algorithm based DE (MSDE) [35], improved whale optimization algorithm (IWOA) [36], self-adaptive gravitational search algorithm and DE (SGSADE) [37], improved dragonfly algorithm (IDA) [38], gbest-guided ABC (GABC) [39], hybrid whale optimization algorithm with DE (WOA-DE) [18], chaotic opposition-based grey wolf optimization algorithm based on DE and disruption operator (COGWO2D) [40], etc.

In fact, there are other types of mutation and crossover operators that have been proposed by researchers to enhance the optimization ability. In 2019, Xu et al. introduced a series of new variants of moth-flame optimization (MFO) by combining MFO with Gaussian mutation (GM), Cauchy mutation (CM), Lévy mutation (LM) or the combination of GM, CM and LM [41]. The experimental results demonstrated that the three strategies can significantly boost exploration and exploitation capabilities of the basic MFO. For the crossover operators, Kita et al. analyzed the unimodal normal distribution crossover (UNDX) by discussing the importance of the distribution and statistics of the offspring yielded by a crossover operator for its evaluation [42]. Akimoto et al. proposed an adaptive real-coded ensemble crossover (AREX) that combines the adaptation of expansion rate technique and the crossover mean descent technique in 2009 [43]. Experimental results showed that the proposed algorithm enlarges the classes of functions that original methods can solve. In 2015, Ariyarit and Kanazaki introduced a modified version of genetic algorithm (GA) with multi-modal distribution crossover (MMDX) [44]. Blend crossover (BLX) [45] and UNDX were used as comparison algorithms. It can be found from the experimental results that MMDX is more competitive and can maintain higher population diversity.

In addition, experiments are performed on eight satellite images (see Figure 5) to determine the optimal parameter settings of the proposed algorithm. The sum of ranks with different combination of α and F is given in Table 1. The lower the ranking value, the better the performance. As can be

observed, $\alpha = 2.5$ and $F = 0.5$ present the best results in most cases, thus this combination of parameter values is adopted in the following experiments.

Table 1. Sum of ranks obtained by the proposed method ($K = 5$) under different of parameter values.

	$F=0.1$	$F=0.3$	$F=0.5$	$F=0.7$	$F=0.9$
$\alpha = 2$	89	41	20	43	109
$\alpha = 2.5$	80	19	9	36	112
$\alpha = 3$	92	65	60	70	115

2.4.3. Algorithm Steps

In this section, a comprehensive algorithm step of DHHO/M based multilevel color image thresholding technique is given in Algorithm 2.

Algorithm 2 Pseudocode of dynamic Harris hawks optimization with a mutation mechanism (DHHO/M) based multilevel color image thresholding

Input: The given color image.

Output: Segmentation thresholds.

```

*****
** Get information about the image **
*****
24. Read the given color image.
25. Extract the histogram of each color component (R, G, and B).
*****
*** Harris Hawks Optimization ***
*****
26. Initialize the position of the hawks  $X_i$  and the rabbit  $X_{rabbit}$ .
27. Initialize the fitness values of the hawks  $f_i$  and the rabbit  $f_{rabbit}$ .
28. Set population size  $N$  and maximum number of iterations  $t_{max}$ .
29. Set the dimensions of the optimization problem  $dim$ , namely the number of thresholds.
30. While (termination condition is not met ( $t < t_{max}$ )) do
31. Check the boundary and evaluate the fitness value of each hawk  $f_i$  using Equations (4)–(6).
32. Update the location  $X_{rabbit}$  and fitness value  $f_{rabbit}$  of rabbit if there is a better one.
33. For (each hawk ( $i = 1 : N$ )) do
34. Update the energy of the rabbit  $E$  using Equation (21). % Dynamic control parameter strategy
35. If ( $|E| \geq 1$ ) then
36. Update the position using Equation (23). % Mutation mechanism
37. Else If ( $|E| < 1$ ) then
38. If ( $r \geq 0.5$  and  $|E| \geq 0.5$ ) then
39. Update the position using Equation (10).
40. Else If ( $r \geq 0.5$  and  $|E| < 0.5$ ) then
41. Update the position using Equation (12).
42. Else If ( $r < 0.5$  and  $|E| \geq 0.5$ ) then
43. Update the position using Equation (16).
44. Else If ( $r < 0.5$  and  $|E| < 0.5$ ) then
45. Update the position using Equation (17).
46. End If
47. End If
48. End For
49. End While

```

Fitness function (Kapur's entropy)

Input: Histogram of a color component, and segmentation thresholds X_i .

Output: Fitness function value f_i .

1. The histogram is divided into $n + 1$ parts by n thresholds.
 2. Calculate the proportion of pixels in each gray level ($p_j, j \in [0, 255]$) to the total based on the histogram.
 3. Compute the sum of the probabilities of the pixels ($\omega_k, k \in [0, n]$) contained in each part.
 4. Calculate the Kapur's entropy of each part ($H_k, k \in [0, n]$).
 5. The sum of the entropies of all parts represents the fitness function value.
 6. $f_i = H_0 + H_1 + \dots + H_n$
-

2.4.4. Computational Complexity

The computational complexity of DHHO/M and HHO algorithms mainly depends on three processes: initialization, function evaluation, and position update. The improvement strategy of this paper only replaces the relevant formulations, and does not add additional judgments, loops or other commands. Therefore, the computational complexity of DHHO/M is approximately the same as that of HHO, which can be computed as follows:

$$\begin{aligned} O(DHHO/M) &= O(\text{initialization}) + O(\text{function evaluation}) + O(\text{position update}) \\ &= O(N) + O(t_{\max} \times N \times Cof) + O(t_{\max} \times N \times dim) \\ &= O(N \times (1 + t_{\max} \times (Cof + dim))), \end{aligned} \quad (24)$$

where N is the size of population, Cof is the cost of function evaluation, dim is the dimension of the given optimization problem, and t_{\max} is the maximum number of the iterations [46].

In fact, the proposed DHHO/M runs slightly faster than the original HHO, which will be demonstrated and analyzed in subsequent experiments.

3. Discussions

3.1. Experimental Setup and Database

In order to assess the performance of the proposed approach, a series of experiments were carried out on various images. More specifically, the experiments can be divided into four parts. For the first part of the experiment, the performance influence of each strategy (dynamic control parameter and mutation mechanism) is investigated, and the relevant algorithms are denoted by DHHO and HHO/M, respectively. Two DHHO variants with different parameter values were also included to further evaluate the effect of the parameter (α). The algorithm with parameter α equal to three is represented as DHHO⁺, and DHHO⁻ indicates $\alpha = 2$. For the second part of the experiment, the proposed method is compared with the traditional HHO and four advanced multilevel thresholding techniques, namely teaching-learning-based optimization (TLBO) [47], whale optimization algorithm with TH heuristic (WOA-TH) [48], improved differential search algorithm (IDSA) [49], and beta differential algorithm (BDE) [50]. The experiment is conducted on eight satellite images (see Figure 5) with low and high threshold levels [51]. For the third part of the experiment, DHHO/M is compared with other thresholding techniques based on different criteria to illustrate its feasibility and universality, such as Tsallis entropy based modified grasshopper optimization algorithm (MGOA) [20] and modified artificial bee colony (MABC) [13], as well as Otsu method based modified flower pollination algorithm (MFPA) [48] and grey wolf optimizer (GWO) [7]. For the fourth part of the experiment, four oil pollution images are used to further evaluate its practicality and feasibility on real engineering problems.

It is worth noting that the parameters of each thresholding method used are the same as the original literature, except for the population size N set to 30 and the number of iterations t_{\max} set to 500 for fair comparison. The parameter setting can be found in Table 2. Besides, the initial population of all algorithms is randomly generated in the solution space, and the termination condition in this work is to reach the maximum number of iterations t_{\max} . A number of 50 independent runs are conducted, and the best result is highlighted in **boldface**. All experiments are executed on a computer with “Microsoft Windows 10” system and “8GB” memory space under Matlab2017.

Table 2. Parameters of the algorithms.

No.	Algorithm	Parameter Setting	Year	Reference
1.	DHHO/M	$\alpha = 2.5, SF = 0.5$	—	—
2.	DHHO	$\alpha = 2.5$ (control parameter)	—	—
3.	HHO/M	$SF = 0.5$ (scaling factor)	—	—
4.	HHO	$E \in [0, 2]$ (energy of a rabbit)	2019	[28]
5.	TLBO	$T_F = 1$ (teaching factor)	2019	[47]
6.	WOA-TH	$G_0 = 40, a_0 = 13$	2019	[48]
7.	IDSA	—	2018	[49]
8.	BDE	$a \in [0, 1]$ (beta distribution parameter)	2018	[52]
9.	MGOA	$\beta = 0.8$ (Levy flight parameter)	2019	[20]
10.	MABC	$K = 300$ (chaotic iteration)	2015	[13]
11.	MFFPA	$p \in [0.2, 0.8]$ (switch possibility)	2018	[53]
12.	GWO	$a \in [0, 2]$ (control parameter)	2017	[7]

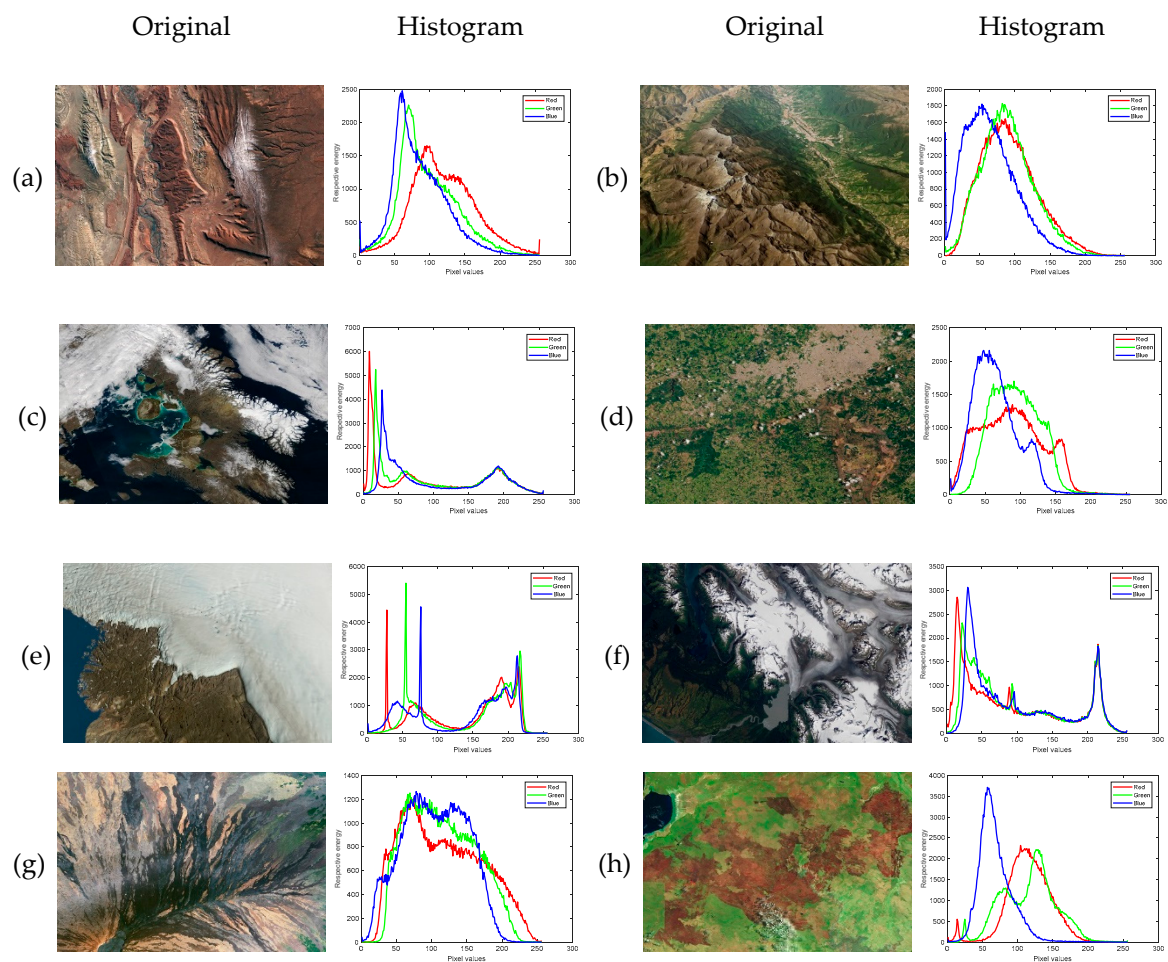


Figure 5. Original satellite images and the corresponding histograms for each of color channels (red, green and blue).

3.2. Performance Metrics.

Several performance metrics are briefed in this section, which can be observed in Table 3. Among the available measures, average fitness function value and standard deviation (Std) are used to evaluate the optimization capability of meta-heuristic algorithm, while peak signal to noise ratio (PSNR), mean squared error (MSE), structural similarity index (SSIM), and feature similarity index (FSIM) are utilized

to assess the quality of the segmented image. Furthermore, Wilcoxon’s rank sum test and Friedman test were adopted for statistical analysis.

Table 3. Performance measures of the multilevel image segmentation methods.

No.	Measures	Formulation	Reference
1.	Average fitness function value	Average = $\frac{\sum_{i=1}^N f_i}{N}$	[40]
2.	Standard deviation (Std)	Std = $\sqrt{\frac{1}{N-1} \sum_{i=1}^N (f_i - \text{Average})^2}$	[46]
3.	Peak signal to noise ratio (PSNR)	PSNR = $10 \log_{10} \left(\frac{255^2}{\text{MSE}} \right)$	[18]
4.	Mean squared error (MSE)	MSE = $\frac{1}{MN} \sum_{i=1}^M \sum_{j=1}^N [I(i, j) - K(i, j)]^2$	[18]
5.	Structural similarity index (SSIM)	SSIM = $\frac{(2\mu_x\mu_y + c_1)(2\sigma_{xy} + c_2)}{(\mu_x^2 + \mu_y^2 + c_1)(\sigma_x^2 + \sigma_y^2 + c_2)}$	[53]
6.	Feature similarity index (FSIM)	FSIM = $\frac{\sum_{x \in \Omega} S_L(x) \cdot PC_m(x)}{\sum_{x \in \Omega} PC_m(x)}$	[23]
7.	Average computation time	Time = $\frac{\sum_{i=1}^N \text{time}_i}{N}$	[17]
8.	Wilcoxon’s rank sum test	$R^+ = \sum_{d_i > 0} \text{rank}(d_i) + \frac{1}{2} \sum_{d_i = 0} \text{rank}(d_i)$ $R^- = \sum_{d_i < 0} \text{rank}(d_i) + \frac{1}{2} \sum_{d_i = 0} \text{rank}(d_i)$	[54]
9.	Friedman test	$F_f = \frac{12n}{k(k+1)} \left[\sum_j R_j^2 - \frac{k(k+1)^2}{4} \right]$	[55]

3.3. Experimental Series 1: Performance on Mathematical Functions

In this section, the proposed algorithm is evaluated on three mathematical test functions with different characteristics, such as unimodal, multi-modal, and composite. The test functions are taken from the CEC2005 special session, which are known as F1, F9, and F14. It can be found from Table 4 (**bold** is the best) that the proposed method outperforms others in most cases, showing its remarkable performance on mathematical test functions. This promising result motivates us to apply it to multilevel image thresholding domain.

Table 4. The experimental results of different algorithms on mathematical test functions.

F		DHHO/M	HHO	TLBO	WOA-TH	IDSA	BDE
F1	Best	6.6218 × 10⁻¹²⁰	5.311 × 10 ⁻¹⁰⁶	54.9103	1.4639	3.4749 × 10 ³	2.7038 × 10 ⁻⁷
	Mean	2.7498 × 10⁻¹⁰⁵	1.7563 × 10 ⁻⁸⁸	4.7014 × 10 ²	2.6078	1.0831 × 10 ⁴	9.2519 × 10 ⁻⁶
	Worst	5.2688 × 10⁻⁹⁷	5.2688 × 10 ⁻⁸⁷	1.4603 × 10 ³	3.5383	2.1372 × 10 ⁴	4.5017 × 10 ⁻⁵
	Std	3.1671 × 10⁻⁹¹	9.6195 × 10 ⁻⁸⁸	3.1022 × 10 ²	0.45694	3.8111 × 10 ³	1.1476 × 10 ⁻⁵
F9	Best	0	0	2.2902 × 10 ²	1.5848 × 10 ²	1.7535 × 10 ²	3.1335 × 10 ⁻⁷
	Mean	0	0	2.7583 × 10 ²	2.1586 × 10 ²	2.0861 × 10 ²	2.1983 × 10 ⁻⁵
	Worst	0	0	3.1682 × 10 ²	2.8732 × 10 ²	2.4096 × 10 ²	1.597 × 10 ⁻⁴
	Std	0	0	23.3213	36.1926	16.7857	3.7214 × 10 ⁻⁵
F14	Best	0.998	0.998	0.998	0.998	0.998	1.0311
	Mean	1.069	1.6254	1.3612	1.1624	2.2329	1.992
	Worst	2.8008	5.9288	5.9288	5.9288	19.2307	0.1815
	Std	0.33043	1.4981	1.5979	0.90024	3.4264	1.3037

3.4. Experimental Series 2: Influence of Dynamic Control Parameter Strategy and Mutation Mechanism

In this section, the influence of each improvement strategy (dynamic control parameter and mutation mechanism) is investigated, and the results can be found in Table 5 (**bold** is the best). As can be observed, DHHO/M presents the highest fitness function value in most cases, while HHO/M and DHHO are ranked second and third respectively. This promising result indicates that introduction of each strategy can improve the performance of the original algorithm, and the combination of them works better. Specifically speaking, the dynamic control parameter strategy prevents falling into local optimum, and the mutation mechanism effectively enhances the global search capability. Thus, DHHO/M exhibits superior performance compared to other algorithms.

Another comparison is made between DHHO, HHO, DHHO⁺, and DHHO⁻. From the table, these algorithms can be arranged as DHHO > HHO ~ DHHO⁺ > DHHO⁻, which strongly supports

the discussion in the previous section. Smaller value of parameter ($\alpha = 2$) makes the amplitude of the disturbance term too large, although the diversity of the population is increased but the algorithm convergence ability is seriously affected. On the contrary, larger value of parameter ($\alpha = 3$) produces a small disturbance. Although the local optimum cannot be avoided, it does not affect the accuracy of the algorithm, so the result is similar to the original algorithm. However, the value of parameter α of DHHO is between the above two, which can enhance the ability to jump out of local optimum while ensuring convergence property, and obtain the best result in this comparison.

Furthermore, the Std values obtained by each algorithm are also given in Table 5. It can be found that DHHO/M presents the lowest value in general, which shows better stability than other algorithms. More detailed and comprehensive stability testing and analysis can be found in the next subsection.

Table 5. The experimental results of HHO variants on satellite images.

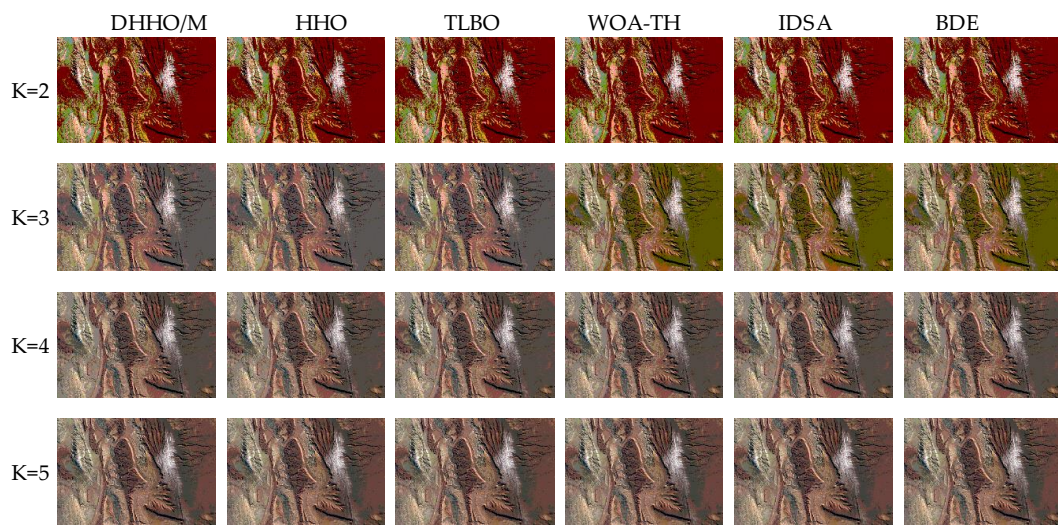
Image	K	DHHO/M		DHHO		HHO/M		HHO		DHHO ⁺		DHHO ⁻	
		Mean	Std	Mean	Std	Mean	Std	Mean	Std	Mean	Std	Mean	Std
1	2	12.6254	0	12.6253	1.00×10^{-4}	12.6254	0	12.6253	1.00×10^{-4}	12.6253	8.46×10^{-5}	12.6217	8.20×10^{-3}
	3	15.9977	1.40×10^{-3}	15.9990	1.70×10^{-3}	15.9990	1.40×10^{-3}	15.9971	1.70×10^{-3}	15.9984	1.80×10^{-3}	15.9981	1.40×10^{-3}
	4	19.1537	0	19.1537	0	19.1537	0	19.1537	0	19.1537	0	19.1537	0
	5	22.0256	2.00×10^{-4}	22.0254	1.00×10^{-4}	22.0254	2.00×10^{-4}	22.0253	5.60×10^{-5}	22.0254	2.00×10^{-4}	22.0254	2.00×10^{-4}
	2	12.6999	0	12.6999	0	12.6999	0	12.6999	0	12.6999	0	12.6999	0
3	3	15.8400	1.30×10^{-3}	15.8400	1.30×10^{-3}	15.8400	1.30×10^{-3}	15.8400	1.60×10^{-3}	15.8400	1.30×10^{-3}	15.8400	1.30×10^{-3}
	4	18.9080	0	18.9080	8.45×10^{-5}	18.9081	2.00×10^{-4}	18.9080	1.00×10^{-4}	18.9080	1.54×10^{-5}	18.9080	2.00×10^{-4}
	5	21.6937	2.16×10^{-5}	21.6589	4.75×10^{-2}	21.6936	2.00×10^{-4}	21.6936	3.07×10^{-5}	21.6936	0.0001	21.6936	1.00×10^{-4}
	2	12.2672	0	12.2672	0	12.2672	0	12.2672	0	12.2672	0	12.2672	0
	3	15.2240	1.99×10^{-2}	15.2388	3.38×10^{-2}	15.2388	1.00×10^{-3}	15.2089	1.71×10^{-2}	15.2314	1.63×10^{-2}	15.2089	1.71×10^{-2}
5	4	18.0756	9.90×10^{-5}	18.0676	1.82×10^{-2}	18.0675	1.81×10^{-2}	18.0599	3.02×10^{-2}	18.0757	1.00×10^{-4}	18.0676	1.82×10^{-2}
	5	20.7387	1.88×10^{-2}	20.7071	5.48×10^{-2}	20.6817	5.05×10^{-2}	20.7265	3.01×10^{-2}	20.7277	3.17×10^{-2}	20.6692	4.47×10^{-2}
	2	12.4226	0	12.4226	0	12.4226	0	12.4226	0	12.4226	0	12.4226	0
	3	15.4792	1.99×10^{-9}	15.4792	1.99×10^{-9}	15.4790	1.99×10^{-9}	15.4792	1.99×10^{-9}	15.4790	1.99×10^{-9}	15.4790	1.99×10^{-9}
	4	18.3182	1.95×10^{-5}	18.3181	5.07×10^{-5}	18.3181	1.95×10^{-5}	18.3181	3.19×10^{-5}	18.3181	2.38×10^{-5}	18.3181	1.95×10^{-5}
7	5	21.0501	3.37×10^{-5}	21.0499	3.00×10^{-4}	21.03316	3.74×10^{-2}	21.0500	2.00×10^{-4}	21.0500	1.00×10^{-4}	20.9918	5.51×10^{-2}
Rank		1(12)		3(8)		2(9)		4(6)		4(6)		6(5)	

3.5. Experimental Series 3: Comparison with Other Advanced Methods on Satellite Images

In this section, the proposed method is compared with other advanced multilevel image segmentation approaches on satellite images. The performance of each algorithm is comprehensively and objectively assessed in terms of precision, stability, statistical significance, scalability (high dimension), and convergence property.

3.5.1. Segmentation Accuracy

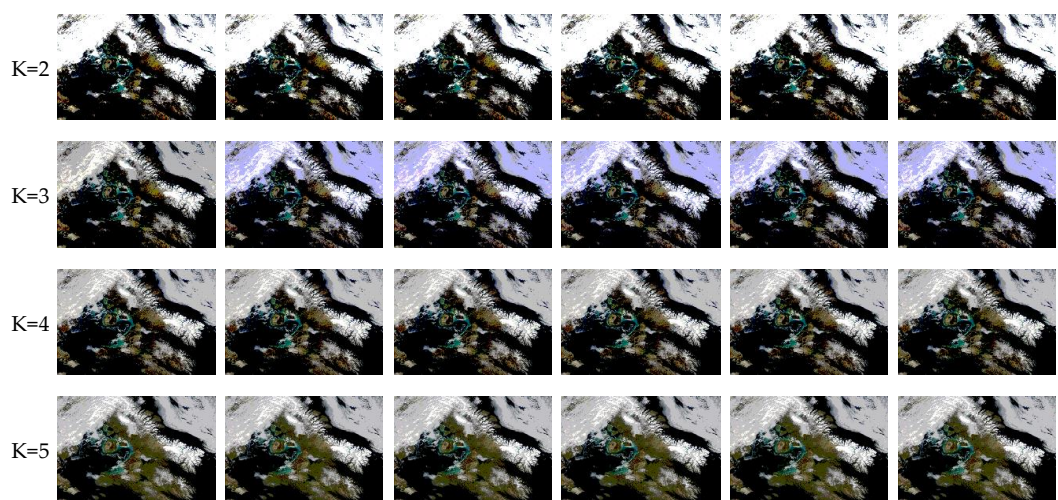
Accuracy is one of the main indicators for measuring image segmentation technique. In this experiment, the precision of each method is evaluated from five aspects, namely average fitness function value, MSE, PSNR, SSIM, and FSIM values. Firstly, the threshold values and segmented images obtained are given in Table 6 and Figure 6, respectively. The threshold levels selected (K = 2, 3, 4, and 5) are the same as [47,49]. As can be observed from Table 6, all methods give similar results when the threshold level is small; while the threshold values determined become different when K = 4 and 5. The reason for this phenomenon is that the difficulty of the current optimization problem increases with the number of thresholds, and some meta-heuristic algorithms with poor search ability are not competent, such as “Image3” at three threshold levels, “Image5” at three threshold levels, and “Image6” at five threshold levels. Considering the segmented images presented in Figure 6, it can be found that the images with high levels contain more information and details than that with low levels, because the of entropy of a given image reflects its average information content [18].



(a) Image1

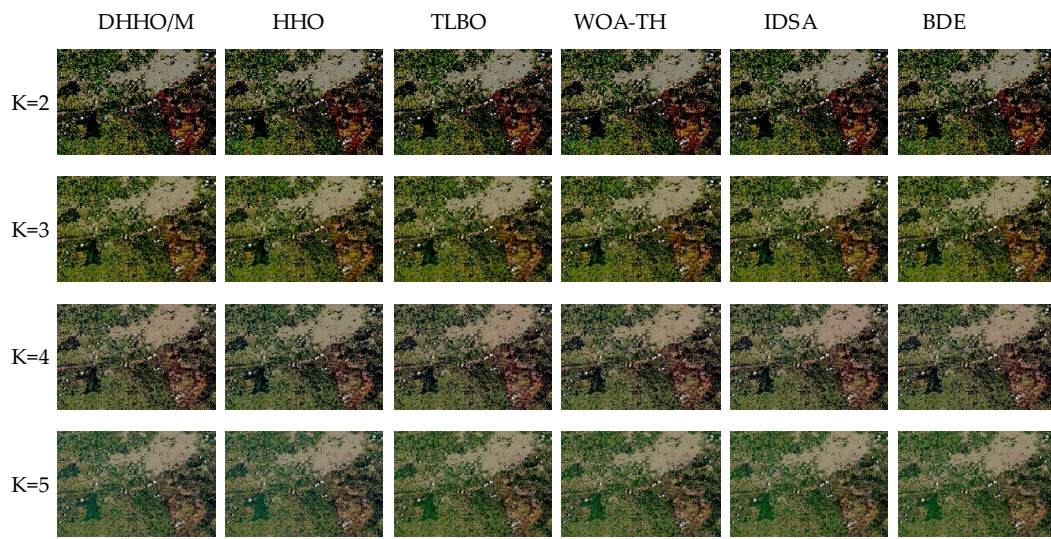


(b) Image2

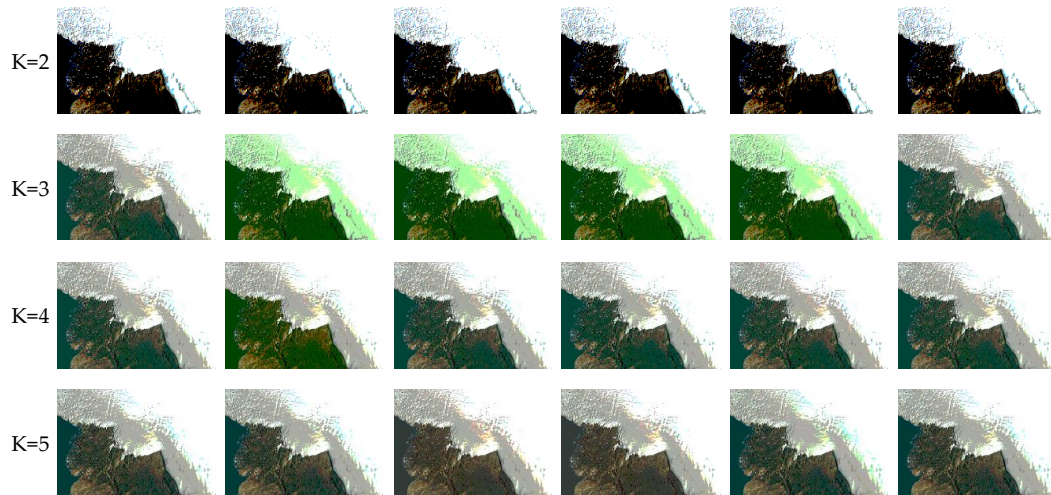


(c) Image3

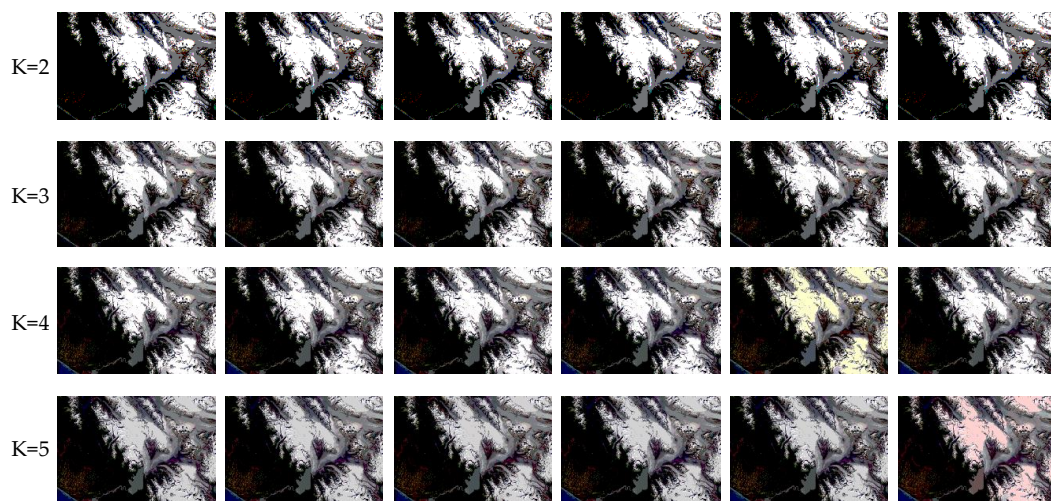
Figure 6. Cont.



(d) Image4



(e) Image5



(f) Image6

Figure 6. Cont.

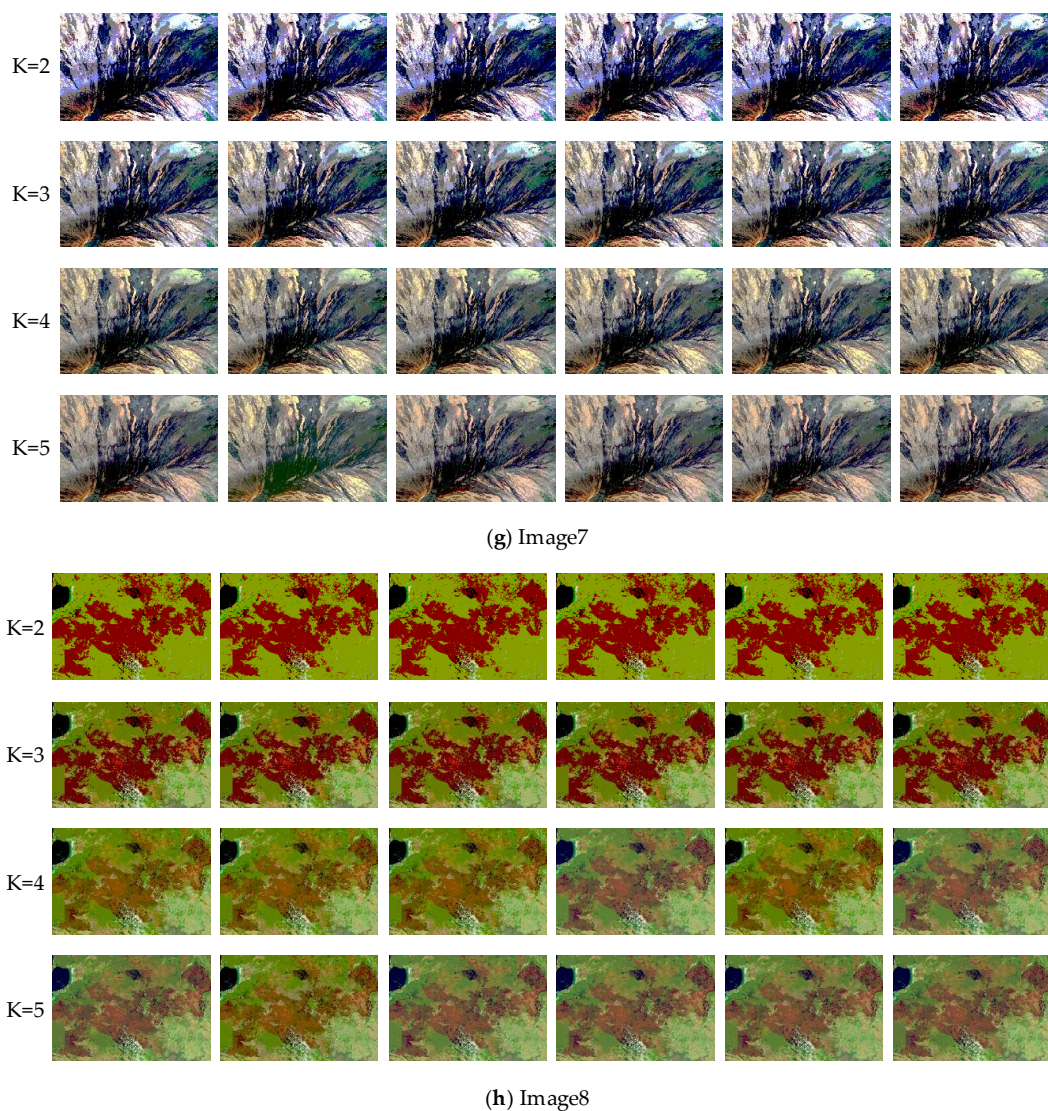


Figure 6. The segmented results of satellite images obtained by different algorithms.

Secondly, the average fitness function values obtained by all algorithms are given in Table 7 (**bold** is the best), which reflects the optimization capability of each meta-heuristic algorithm. Higher Kapur's entropy value indicates stronger search ability and higher precision. It can be observed that the values of all algorithms increase with the number of threshold levels, and DHHO/M outperforms other compared methods in general. This results strongly proves that high-quality segmented image with more information can be obtained at higher threshold level, such as $K = 5$. In DHHO/M, the introduction of dynamic control parameter strategy and mutation mechanism can improve the search efficiency of the algorithm and avoid premature convergence. Therefore, the superiority of the proposed algorithm is holistic rather than on a single image.

Thirdly, several performance metrics are introduced to assess the similarity between the segmented image and the original image, such as PSNR, MSE, SSIM, and FSIM. The experimental results are given in two tables. In Table 8, it can be found that the PSNR value increases with the number of threshold values, while MSE value is the opposite (**bold** is the best). Similarly, SSIM and FSIM values also increase with the number of threshold levels, as can be seen from Table 9 (**bold** is the best). These promising phenomena indicate that the quality of segmented image is improving gradually; while the results obtained by the proposed method are better than or at least comparable to other approaches, showing better feature and structure preserving ability.

Table 6. Comparison of optimal thresholds for different algorithms using Kapur’s entropy at 2– 5 levels.

Image	K	DHHO/M			HHO			TLBO		
		R	G	B	R	G	B	R	G	B
1	2	58,171	111,189	117,187	58,171	111,189	117,187	58,171	111,189	117,187
	3	56,123,188	48,122,192	42,128,191	56,123,188	48,122,192	42,128,191	56,123,188	48,122,192	85,143,203
	4	53,110,163,209	45,102,156,207	41,95,149,203	53,110,163,209	45,102,156,207	41,95,149,203	53,110,163,209	45,102,156,207	41,95,149,203
2	5	45,86,130,173,213	44,90,133,174,216	37,85,129,170,210	42,82,126,171,213	44,90,133,174,216	37,85,130,171,210	42,82,126,171,213	44,90,133,174,216	37,85,129,170,210
	2	94,164	98,168	80,146	94,164	98,168	80,146	94,164	98,168	80,146
	3	78,141,199	66,132,192	70,131,185	78,141,199	66,132,192	70,131,185	78,141,199	66,132,192	70,131,185
3	4	67,120,169,217	57,107,152,195	53,102,148,200	67,120,169,217	57,107,152,195	56,107,154,200	67,120,169,217	57,107,152,195	53,102,148,200
	5	53,97,140,180,220	55,101,145,186,222	45,87,128,167,202	53,97,140,180,220	55,101,145,186,222	44,85,126,167,202	53,96,138,180,220	55,101,145,186,222	44,85,126,167,202
	2	86,163	85,162	80,162	86,163	85,162	80,162	86,163	85,162	80,162
4	3	84,152,207	81,150,207	65,117,170	84,152,207	81,150,207	78,152,210	84,152,207	81,150,207	65,117,170
	4	70,117,165,216	69,117,166,216	65,114,165,218	70,117,165,216	67,115,165,216	65,114,165,218	70,117,165,216	69,117,166,216	65,114,165,218
	5	36,82,125,168,216	45,85,126,168,216	57,93,132,171,218	36,82,125,168,216	45,85,126,168,216	18,65,114,165,218	36,82,125,168,216	45,85,126,168,216	58,95,134,172,218
5	2	92,179	96,171	82,146	92,179	96,171	82,146	92,179	96,171	82,146
	3	63,120,182	72,118,171	79,137,176	63,120,182	72,118,171	79,137,176	63,120,182	72,118,171	79,137,176
	4	47,89,132,182	70,114,159,194	50,91,137,176	47,89,132,182	70,114,159,194	50,91,137,176	47,89,132,182	70,114,159,194	50,91,137,176
6	5	46,87,129,176,209	52,88,124,164,205	31,66,99,142,183	46,87,129,176,209	49,86,123,164,205	49,90,134,162,198	46,87,129,176,209	48,85,122,164,205	47,91,136,164,198
	2	97,158	95,156	81,144	97,158	95,156	81,144	97,158	95,156	81,144
	3	97,148,183	38,96,156	83,138,181	97,148,183	38,96,156	28,82,144	97,148,183	96,150,187	83,138,180
7	4	74,109,150,184	40,96,150,187	28,83,138,181	74,109,150,184	38,96,150,187	28,83,138,181	78,112,150,184	38,96,150,187	28,83,138,181
	5	64,93,121,153,186	38,79,112,152,188	24,52,88,138,181	64,93,121,153,186	38,82,114,152,188	28,80,112,144,183	20,74,109,148,183	38,79,112,152,188	28,80,112,144,183
	2	74,150	77,152	80,154	74,150	77,152	80,154	74,150	77,152	80,154
8	3	62,122,183	68,129,187	72,130,187	62,122,183	68,129,187	72,130,187	62,122,183	68,129,187	72,130,187
	4	51,98,147,194	61,105,151,197	61,106,152,197	51,98,147,194	61,105,151,197	61,106,152,197	51,98,147,194	61,105,151,197	61,106,152,197
	5	49,95,143,190,228	61,103,148,191,228	58,102,148,191,227	49,95,143,190,228	61,103,148,191,228	58,102,148,191,227	50,95,145,191,230	61,103,148,191,228	60,106,152,194,227
9	2	96,169	97,160	64,129	96,169	97,160	64,129	96,169	97,160	64,129
	3	80,135,190	81,129,177	55,105,154	80,135,190	81,129,177	55,105,154	80,135,190	81,129,177	55,105,154
	4	67,113,159,204	69,108,148,188	54,101,148,197	68,114,159,204	69,108,148,188	54,101,148,197	67,113,159,204	69,108,148,188	54,101,148,197
10	5	57,94,132,171,209	68,107,146,185,226	48,87,125,163,197	57,94,132,171,209	24,70,110,149,188	50,90,129,168,206	15,68,114,159,204	68,107,146,185,226	48,87,125,163,197
	2	71,197	111,203	125,168	71,197	111,203	126,179	71,197	111,203	126,179
	3	70,138,197	96,150,204	84,132,179	70,138,197	96,150,204	26,86,142	70,138,197	96,150,204	84,132,179
11	4	69,114,155,197	56,106,152,204	26,84,132,179	69,114,155,197	56,106,152,204	27,84,132,179	69,114,155,197	54,105,152,204	26,85,132,179
	5	69,111,151,189,219	54,97,138,171,207	26,82,126,163,203	69,111,151,189,219	54,97,138,171,207	26,82,126,163,199	69,111,151,189,219	56,105,148,189,215	26,82,126,163,203

Table 6. Cont.

Image	K	WOA-TH			IDSA			BDE		
		R	G	B	R	G	B	R	G	B
1	2	58,171	111,189	117,187	58,171	111,189	117,187	58,171	111,189	117,187
	3	56,123,188	48,122,192	84,142,203	56,123,188	48,122,192	85,143,203	56,123,188	48,122,192	85,143,203
	4	53,110,163,209	45,102,156,207	41,95,149,203	53,110,163,209	45,102,156,207	41,94,149,203	53,111,162,209	45,102,156,207	41,95,149,203
2	5	42,82,126,171,213	44,90,133,174,216	37,85,129,170,210	45,86,128,171,211	44,90,133,174,214	40,89,133,172,210	42,82,126,171,213	44,90,133,174,216	37,85,129,170,210
	2	94,164	98,168	80,146	94,164	98,168	80,146	94,164	98,168	80,146
	3	78,141,199	66,132,192	70,131,185	78,141,199	66,132,192	70,131,185	78,141,199	66,132,192	70,131,185
3	4	67,120,169,217	57,107,152,195	57,109,154,200	60,109,155,199	57,107,152,195	56,107,154,200	67,120,169,217	57,107,152,195	53,102,148,200
	5	53,96,138,180,220	55,101,145,186,222	45,88,131,169,202	53,95,137,180,220	53,97,138,178,215	45,87,128,167,202	52,93,134,174,217	55,101,145,186,222	42,84,126,167,202
	2	86,163	85,162	80,162	86,163	85,162	80,162	86,163	85,162	80,162
4	3	84,152,207	81,150,207	65,117,170	84,152,207	81,150,207	78,152,210	84,152,207	81,150,207	65,117,170
	4	70,117,165,216	69,117,166,216	65,114,165,218	70,117,165,216	69,117,166,216	65,115,165,218	70,117,165,216	69,117,166,216	65,114,165,218
	5	36,82,125,168,216	45,85,126,168,216	58,95,134,172,218	34,81,123,167,216	45,85,126,168,216	58,95,133,171,218	36,82,125,168,216	45,85,126,168,216	58,95,134,172,218
5	2	92,179	96,171	82,146	92,179	96,171	82,146	92,179	96,171	82,146
	3	63,120,182	72,118,171	79,137,176	62,120,182	72,118,171	79,137,176	63,120,182	72,118,171	79,137,176
	4	47,89,132,182	71,115,164,205	50,91,137,176	62,118,176,209	70,114,159,194	50,91,137,176	47,89,132,182	70,113,158,194	50,91,137,176
6	5	47,89,130,176,209	49,86,123,164,205	49,90,134,162,198	42,84,124,176,209	48,85,121,159,194	49,90,134,162,197	46,88,130,176,209	52,87,122,160,198	49,90,134,162,198
	2	97,158	95,156	81,144	97,158	95,156	81,144	97,158	95,157	81,144
	3	97,148,183	38,96,156	83,138,181	97,148,183	38,96,156	83,138,181	97,148,183	39,96,156	83,138,181
7	4	74,109,150,184	38,96,150,187	28,83,138,181	74,109,150,184	38,96,150,187	28,83,138,180	74,109,150,184	38,96,150,187	28,83,138,182
	5	21,78,112,150,184	38,82,114,152,188	28,80,112,144,183	21,78,112,150,184	38,79,113,151,188	28,80,112,144,181	21,74,109,150,184	38,79,112,152,188	30,83,113,156,197
	2	74,150	77,152	80,154	74,150	77,152	80,154	74,150	77,152	80,154
8	3	62,122,183	68,129,187	72,130,187	62,122,183	68,129,187	72,131,187	64,125,184	68,129,187	72,130,187
	4	51,98,147,194	61,105,151,197	61,106,152,197	52,99,147,194	61,105,151,196	62,107,152,198	51,98,147,194	61,105,151,197	61,106,152,197
	5	49,95,143,190,228	61,103,148,191,228	58,102,148,191,227	55,99,146,190,228	61,103,148,191,228	51,86,123,161,200	49,95,143,190,228	61,103,148,191,228	58,102,148,191,227
9	2	96,169	97,160	64,129	96,169	97,160	64,129	96,169	97,160	64,129
	3	80,135,190	81,129,177	55,105,154	80,135,190	81,129,177	55,105,154	80,135,190	81,129,177	55,105,154
	4	68,114,159,204	70,110,149,188	54,101,148,197	68,114,159,204	69,108,148,188	54,101,148,197	67,113,159,204	69,108,148,188	54,101,148,197
10	5	57,94,132,171,209	68,107,146,185,226	50,90,129,168,206	58,96,134,172,211	68,107,146,185,226	48,86,124,163,197	57,94,132,171,209	68,107,146,185,226	48,87,125,163,197
	2	71,197	111,203	126,179	71,197	111,203	126,179	71,197	111,203	126,179
	3	70,138,197	96,150,204	84,132,179	70,138,197	96,150,204	84,132,179	70,138,197	96,150,204	84,132,179
11	4	69,114,155,197	56,106,152,204	26,84,132,179	69,115,157,198	56,106,152,204	79,125,163,203	69,114,155,197	56,106,152,204	79,120,152,193
	5	69,111,151,189,219	56,104,146,189,215	26,79,120,152,193	68,111,151,189,219	53,86,119,158,204	26,79,120,152,193	69,111,151,189,219	54,103,148,190,216	27,82,125,163,199

Table 7. The average fitness values and std values of different algorithms at 2, 3, 4, and 5 levels.

Image	K	DHHO/M		HHO		TLBO		WOA-TH		IDSA		BDE	
		Mean	Std										
1	2	12.6254	3.68×10^{-9}	12.6254	4.73×10^{-3}	12.6254	3.68×10^{-9}	12.6254	3.68×10^{-9}	12.6254	1.20×10^{-5}	12.6254	3.68×10^{-9}
	3	15.9965	1.31×10^{-3}	15.9996	1.61×10^{-3}	15.9996	1.67×10^{-3}	15.9996	1.31×10^{-3}	15.9997	1.52×10^{-3}	15.9997	1.61×10^{-3}
	4	19.1537	1.49×10^{-4}	19.1537	3.86×10^{-5}	19.1537	3.63×10^{-4}	19.1537	3.68×10^{-9}	19.153	6.46×10^{-4}	19.1523	5.59×10^{-3}
	5	22.0256	1.15×10^{-4}	22.0251	2.11×10^{-4}	22.0256	2.40×10^{-4}	22.025	3.54×10^{-4}	22.0236	2.26×10^{-3}	21.9903	1.42×10^{-2}
2	2	12.2446	3.68×10^{-9}	12.2446	1.61×10^{-4}	12.2446	3.68×10^{-9}	12.2446	3.68×10^{-9}	12.2446	3.68×10^{-9}	12.2446	2.78×10^{-4}
	3	15.4553	1.51×10^{-4}	15.4553	2.03×10^{-4}	15.4553	1.92×10^{-5}	15.4553	2.03×10^{-4}	15.4553	9.03×10^{-4}	15.4553	4.76×10^{-3}
	4	18.4839	1.84×10^{-4}	18.4835	2.90×10^{-4}	18.4839	4.84×10^{-4}	18.4833	1.86×10^{-4}	18.4813	2.30×10^{-3}	18.4839	3.16×10^{-2}
	5	21.3181	1.64×10^{-4}	21.3179	2.35×10^{-3}	21.318	2.65×10^{-3}	21.3178	1.02×10^{-3}	21.3125	1.27×10^{-2}	21.3156	6.00×10^{-3}
3	2	12.6999	1.84×10^{-9}	12.6999	5.73×10^{-5}								
	3	15.8406	4.84×10^{-5}	15.8377	1.00×10^{-3}	15.8406	7.36×10^{-4}	15.8406	1.18×10^{-3}	15.8377	2.55×10^{-3}	15.8406	1.00×10^{-3}
	4	18.9081	4.91×10^{-5}	18.9079	6.67×10^{-4}	18.9081	0	18.9081	4.89×10^{-5}	18.908	2.96×10^{-3}	18.9081	3.40×10^{-3}
	5	21.6937	2.00×10^{-5}	21.609	2.98×10^{-2}	21.6934	3.81×10^{-5}	21.6937	7.03×10^{-4}	21.6935	1.19×10^{-3}	21.6937	2.49×10^{-3}
4	2	12.458	3.68×10^{-9}	12.458	3.68×10^{-9}	12.458	4.04×10^{-5}	12.458	3.68×10^{-9}	12.458	2.12×10^{-5}	12.458	1.21×10^{-3}
	3	15.5803	3.68×10^{-9}	15.5803	3.68×10^{-9}	15.5803	3.05×10^{-5}	15.5803	3.68×10^{-9}	15.5803	3.06×10^{-3}	15.5803	3.07×10^{-4}
	4	18.4835	9.69×10^{-4}	18.4834	1.39×10^{-3}	18.4834	1.56×10^{-3}	18.4834	8.01×10^{-5}	18.4806	1.26×10^{-3}	18.4814	7.04×10^{-4}
	5	21.2255	5.82×10^{-3}	21.2089	8.52×10^{-3}	21.2211	5.99×10^{-3}	21.2254	6.81×10^{-3}	21.2155	1.02×10^{-2}	21.2211	6.13×10^{-3}
5	2	12.2672	1.84×10^{-9}	12.2665	1.84×10^{-9}								
	3	15.2393	1.12×10^{-3}	15.2023	1.93×10^{-2}	15.1498	1.67×10^{-2}	15.2393	1.30×10^{-2}	15.2393	1.30×10^{-2}	15.2383	1.32×10^{-3}
	4	18.0758	1.63×10^{-2}	18.0758	2.38×10^{-2}	18.0756	1.24×10^{-4}	18.0758	1.47×10^{-2}	18.0757	3.41×10^{-2}	18.0754	5.10×10^{-3}
	5	20.7597	1.78×10^{-2}	20.6966	4.23×10^{-2}	20.7506	2.79×10^{-2}	20.6622	3.78×10^{-2}	20.7588	3.35×10^{-2}	20.6768	3.75×10^{-2}
6	2	12.6459	3.68×10^{-9}	12.6459	5.35×10^{-6}	12.6459	3.16×10^{-5}						
	3	15.8348	3.68×10^{-9}	15.8348	5.86×10^{-5}	15.8346	7.96×10^{-4}						
	4	18.8099	6.43×10^{-6}	18.8099	6.43×10^{-6}	18.8099	4.23×10^{-5}	18.8099	3.03×10^{-5}	18.8089	5.43×10^{-4}	18.8099	1.48×10^{-3}
	5	21.5849	7.36×10^{-5}	21.5849	1.47×10^{-4}	21.5817	8.43×10^{-3}	21.5849	7.23×10^{-5}	21.5556	1.26×10^{-2}	21.5849	1.02×10^{-2}
7	2	12.4226	3.68×10^{-9}	12.4226	3.98×10^{-5}								
	3	15.4792	5.52×10^{-9}	15.4792	5.37×10^{-5}	15.4792	4.44×10^{-5}						
	4	18.3182	2.12×10^{-5}	18.3181	2.41×10^{-2}	18.3182	6.18×10^{-5}	18.3181	2.84×10^{-5}	18.3181	4.27×10^{-3}	18.3182	3.07×10^{-3}
	5	21.0502	7.07×10^{-5}	20.9663	3.46×10^{-2}	20.9277	6.17×10^{-4}	21.0501	2.16×10^{-2}	21.0492	2.60×10^{-2}	21.0502	3.01×10^{-2}
8	2	12.0856	1.33×10^{-4}	12.0853	2.78×10^{-3}	12.0853	1.75×10^{-3}	12.0853	1.33×10^{-5}	12.0853	1.77×10^{-3}	12.0853	8.05×10^{-4}
	3	15.3334	5.52×10^{-9}	15.1937	3.60×10^{-2}	15.3334	5.52×10^{-9}	15.3334	5.52×10^{-9}	15.3334	9.91×10^{-4}	15.3334	4.08×10^{-4}
	4	18.2572	7.30×10^{-4}	18.256	5.24×10^{-3}	18.2552	1.02×10^{-3}	18.2562	4.88×10^{-4}	18.2573	2.32×10^{-3}	18.2547	2.94×10^{-3}
	5	21.0181	1.25×10^{-3}	21.0155	3.78×10^{-2}	21.0173	1.49×10^{-3}	21.0142	3.70×10^{-2}	21.0163	1.57×10^{-2}	21.0136	2.38×10^{-3}

Table 8. The PSNR values and MSE values of different algorithms at 2, 3, 4, and 5 levels.

Image	K	DHHO/M		HHO		TLBO		WOA-TH		IDSA		BDE	
		PSNR	MSE										
1	2	13.4568	3409.6288	13.5059	3409.6288	13.4568	3409.6288	13.4568	3409.6288	13.4568	3409.6288	13.4568	3409.6288
	3	20.8043	541.7281	18.7437	541.7281	18.7437	1101.2048	18.7437	1079.8563	18.8912	1101.2048	18.8668	1101.2048
	4	23.5379	286.5668	23.5379	288.2504	23.5379	288.2504	23.5379	288.2504	23.4893	286.8563	23.4844	288.2504
	5	25.3432	190.0378	25.2873	190.4263	25.3432	190.0378	25.2458	190.0378	25.3091	199.5299	24.8902	192.3651
2	2	13.761	2793.6353										
	3	17.1656	1274.8825										
	4	19.8508	690.9693	19.6349	725.6155	19.8508	690.9693	19.5626	738.4191	20.126	638.7005	19.8508	690.9693
	5	22.2059	393.4485	21.9532	415.6597	21.962	414.8152	21.8581	424.2548	22.073	403.525	21.8664	423.4967
3	2	14.6099	2250.563										
	3	17.7343	1096.4772	17.0737	1316.3943	17.0737	1316.3943	17.0737	1316.3943	17.7343	1096.4772	17.0737	1316.3943
	4	19.5277	729.8596	19.4491	743.2218	19.4491	743.2218	19.4491	743.2218	19.4482	743.4005	19.4491	743.2218
	5	24.4587	238.8742	22.7205	395.9433	22.6857	401.4084	22.6857	401.4084	22.6956	401.0393	22.6857	401.4084
4	2	14.1596	2518.0049										
	3	17.3051	1316.1756	17.3051	1316.1756	17.3051	1316.1756	17.3051	1316.1756	17.3486	1308.8014	17.3051	1316.1756
	4	20.3568	652.8288	20.3524	653.8501	20.3524	653.8501	20.2761	672.0299	19.4048	764.8489	20.3524	653.8501
	5	24.0586	266.308	22.6141	375.5379	22.8347	354.1505	22.5577	379.7771	22.9103	356.3137	22.3481	392.8026
5	2	12.3149	3817.5316	12.3149	3817.5316	12.3149	3817.5316	12.3149	3817.5316	12.3149	3817.5316	12.3247	3809.1362
	3	14.3753	2377.2328	13.9334	2642.1422	14.3388	2396.5364	14.3753	2377.2328	14.3753	2377.2328	14.3747	2377.5557
	4	16.904	1355.9069	16.8586	1368.8135	16.7536	1413.0432	16.8586	1368.8135	16.8158	1381.3574	16.8516	1370.5727
	5	18.529	941.6725	17.4932	1166.1194	17.6121	1131.203	17.661	1117.2575	17.5692	1142.5529	17.4611	1174.9531
6	2	15.4096	1875.6465										
	3	17.3586	1204.8869	17.3586	1204.8869	17.3586	1204.8869	17.3586	1204.8869	17.3576	1205.2089	17.3217	1213.4404
	4	18.6145	906.6325	18.6145	906.6325	18.6145	906.6325	18.6145	906.6325	18.5634	916.8623	18.6145	906.6325
	5	20.6141	586.8374	20.6141	586.8374	20.4926	603.118	20.6141	586.8374	20.1165	651.1384	20.6141	586.8374
7	2	12.9658	3316.6781										
	3	16.2594	1542.3302										
	4	19.9285	710.127	19.8763	720.2965	19.9285	710.127	19.8208	732.3273	19.8763	720.2965	19.9285	710.127
	5	22.7765	353.4079	21.725	476.8748	22.5737	406.4345	21.5981	484.4584	21.6863	481.3556	21.725	476.8748
8	2	14.2476	2953.5281	14.2452	2956.1504	14.2452	2956.1504	14.2452	2956.1504	14.2452	2956.1504	14.2452	2956.1504
	3	18.4536	854.9528	16.9544	1753.3657	16.9544	1753.3657	16.9544	1753.3657	16.9544	1753.3657	16.9544	1753.3657
	4	24.6745	222.5721	24.5916	227.417	24.5902	227.4794	24.5902	227.4794	20.7867	1039.7204	20.8096	1035.361
	5	25.5344	183.0689	25.2902	193.2529	25.0615	204.0797	25.1686	199.832	25.2937	193.1147	25.1855	198.1814

Table 9. The SSIM values and FSIM values of different algorithms at 2, 3, 4, and 5 levels.

Image	K	DHHO/M		HHO		TLBO		WOA-TH		IDSA		BDE	
		SSIM	FSIM										
1	2	0.3288	0.5472	0.3319	0.549	0.3288	0.5472	0.3288	0.5472	0.3288	0.5472	0.3288	0.5472
	3	0.5893	0.7387	0.57	0.7148	0.57	0.7148	0.57	0.7148	0.577	0.7203	0.5776	0.7205
	4	0.7415	0.827	0.7415	0.827	0.7415	0.827	0.7415	0.827	0.7415	0.8269	0.7407	0.8261
	5	0.7945	0.8763	0.7945	0.8761	0.7945	0.8761	0.7917	0.8738	0.794	0.8755	0.7838	0.866
2	2	0.2696	0.5527										
	3	0.4376	0.6476										
	4	0.5737	0.7436	0.5634	0.7323	0.5737	0.7382	0.56	0.73	0.5829	0.7382	0.5737	0.7382
	5	0.6669	0.7981	0.6577	0.7928	0.6584	0.7936	0.6536	0.79	0.663	0.7965	0.6543	0.7902
3	2	0.3643	0.6627										
	3	0.4218	0.7239	0.4209	0.7217	0.4218	0.7217	0.4218	0.7217	0.4209	0.7239	0.4218	0.7217
	4	0.4886	0.7808	0.4863	0.7801	0.4863	0.7801	0.4863	0.7801	0.4864	0.78	0.4863	0.7801
	5	0.6693	0.8431	0.5795	0.837	0.5785	0.837	0.5785	0.837	0.5788	0.837	0.5785	0.837
4	2	0.4043	0.6463										
	3	0.5746	0.7584	0.5734	0.758	0.5734	0.758	0.5734	0.758	0.5734	0.758	0.5734	0.758
	4	0.7328	0.8331	0.7323	0.8331	0.7323	0.8331	0.7291	0.832	0.698	0.813	0.7323	0.8336
	5	0.8336	0.8869	0.792	0.8683	0.7966	0.8692	0.7909	0.8678	0.7978	0.8711	0.7883	0.8655
5	2	0.4806	0.6389	0.4802	0.6385								
	3	0.5432	0.67	0.619	0.6865	0.4693	0.6537	0.5432	0.67	0.5432	0.67	0.5435	0.67
	4	0.6459	0.7142	0.6454	0.7138	0.6398	0.7117	0.6454	0.7138	0.6459	0.7137	0.6456	0.714
	5	0.694	0.7515	0.679	0.7417	0.7136	0.7506	0.7093	0.7474	0.7109	0.7485	0.7132	0.7504
6	2	0.4053	0.6628										
	3	0.4741	0.7409	0.4741	0.7409	0.4741	0.7409	0.4741	0.7409	0.474	0.7408	0.4717	0.74
	4	0.5283	0.7827	0.5283	0.7827	0.5283	0.7827	0.5283	0.7827	0.5259	0.7822	0.5283	0.7827
	5	0.5595	0.8096	0.5589	0.8092	0.5548	0.8075	0.5589	0.8092	0.5589	0.8092	0.5589	0.8092
7	2	0.4061	0.6178										
	3	0.5456	0.7131										
	4	0.6569	0.7859	0.6557	0.7858	0.6569	0.7859	0.654	0.7853	0.6557	0.7858	0.6569	0.7859
	5	0.7557	0.8372	0.7234	0.829	0.7434	0.8306	0.7194	0.8261	0.7219	0.8282	0.7234	0.829
8	2	0.2264	0.4841	0.2261	0.484	0.2261	0.484	0.2261	0.484	0.2261	0.484	0.2261	0.484
	3	0.5319	0.659	0.3864	0.6196	0.3864	0.6196	0.3864	0.6196	0.3864	0.6196	0.3864	0.6196
	4	0.6547	0.7485	0.6539	0.7473	0.6532	0.7458	0.6539	0.7473	0.5122	0.7049	0.5152	0.7099
	5	0.6961	0.7923	0.6829	0.777	0.6724	0.7666	0.6804	0.7752	0.6829	0.7771	0.6744	0.7686

3.5.2. Statistical Test

The experiments performed by each algorithm are the same, so the statistical test is necessary. Parametric statistical test is based on various assumptions, such as independence, normality, and synchronization [56]. However, these assumptions probably not valid when analyzing meta-heuristic algorithms with stochastic property. Therefore, two famous nonparametric statistical tests are adopted in this study, namely, Wilcoxon’s rank sum test [54] and Friedman test [55]. As a brief review, the null hypothesis (H_0) assumes that there is no difference between the two compared algorithms (Wilcoxon’s rank sum test) or the whole (Friedman test); while the alternative hypothesis H_1 indicates the difference. More detailed discussion of these two statistical tests can be found in [55].

The experimental results are given in three tables. Table 10 presents the p-values and h-values of Wilcoxon’s rank sum test obtained by each comparison. It can be found that DHHO/M gives better results in 29 out of 32 cases (eight images and four threshold levels) for HHO, 30 cases for TLBO, 31 cases for WOA-TH, 30 cases for IDSA, and 30 cases for BDE, which shows significant difference between the proposed method and other approaches. As for the average rank of Friedman test given in Table 11, the proposed method ranks first in all cases, and the value of rank becomes smaller as the number of threshold level increases, indicating greater advantages over other compared methods (**bold** is the best). Table 12 gives the Chi-square (χ^2) value and p-value of Friedman test at different threshold levels. According to the Chi-square distribution table, the critical value for 5 (6 algorithm - 1) degrees of freedom at 0.05 significant level is 11.07 [57]. It can be observed from the table that the Chi-square values obtained are much larger than the critical value and the p-values obtained are much smaller than the significant level. The results illustrate that the advantage of the proposed algorithm becomes more obvious as the dimension of the optimization problem increases, and there is a significant difference between the available methods.

Table 10. Results of Wilcoxon’s rank sum test over all available satellite images at 2, 3, 4, and 5 levels.

Image	K	DHHO/M versus									
		HHO		TLBO		WOA-TH		IDSA		BDE	
		p	h	p	h	p	h	p	h	p	h
1	2	<0.05	1	<0.05	1	0.4197	0	<0.05	1	<0.05	1
	3	<0.05	1	<0.05	1	<0.05	1	<0.05	1	<0.05	1
	4	<0.05	1	<0.05	1	<0.05	1	0.0957	0	<0.05	1
	5	<0.05	1	<0.05	1	<0.05	1	<0.05	1	<0.05	1
2	2	<0.05	1	<0.05	1	<0.05	1	<0.05	1	<0.05	1
	3	<0.05	1	<0.05	1	<0.05	1	<0.05	1	0.0784	0
	4	0.0692	0	<0.05	1	<0.05	1	<0.05	1	<0.05	1
3	2	<0.05	1	<0.05	1	<0.05	1	<0.05	1	<0.05	1
	3	<0.05	1	<0.05	1	<0.05	1	<0.05	1	<0.05	1
	4	<0.05	1	0.2117	0	<0.05	1	<0.05	1	<0.05	1
	5	<0.05	1	<0.05	1	<0.05	1	<0.05	1	<0.05	1
4	2	<0.05	1	<0.05	1	<0.05	1	<0.05	1	<0.05	1
	3	<0.05	1	<0.05	1	<0.05	1	<0.05	1	<0.05	1
	4	<0.05	1	<0.05	1	<0.05	1	<0.05	1	<0.05	1
5	2	<0.05	1	<0.05	1	<0.05	1	<0.05	1	<0.05	1
	3	<0.05	1	<0.05	1	<0.05	1	<0.05	1	<0.05	1
	4	<0.05	1	<0.05	1	<0.05	1	0.2624	0	<0.05	1
	5	<0.05	1	<0.05	1	<0.05	1	<0.05	1	<0.05	1
6	2	<0.05	1	<0.05	1	<0.05	1	<0.05	1	<0.05	1
	3	<0.05	1	0.0544	0	<0.05	1	<0.05	1	<0.05	1
	4	<0.05	1	<0.05	1	<0.05	1	<0.05	1	0.1342	0
	5	0.2744	0	<0.05	1	<0.05	1	<0.05	1	<0.05	1
7	2	<0.05	1	<0.05	1	<0.05	1	<0.05	1	<0.05	1
	3	<0.05	1	<0.05	1	<0.05	1	<0.05	1	<0.05	1
	4	<0.05	1	<0.05	1	<0.05	1	<0.05	1	<0.05	1
8	2	<0.05	1	<0.05	1	<0.05	1	<0.05	1	<0.05	1
	3	0.0963	0	<0.05	1	<0.05	1	<0.05	1	<0.05	1
	4	<0.05	1	<0.05	1	<0.05	1	<0.05	1	<0.05	1
	5	<0.05	1	<0.05	1	<0.05	1	<0.05	1	<0.05	1

Table 11. Friedman rank of different algorithms considering all experimental data at 2, 3, 4, and 5 levels.

K	DHHO/M	HHO	TLBO	WOA-TH	IDSA	BDE
2	3.10417	3.44792	3.53125	3.41667	3.63542	3.86458
3	2.39583	3.85417	3.83333	3.41667	3.60417	3.89583
4	1.93750	3.61458	3.36458	3.61458	4.67708	3.79167
5	1.29167	3.84375	3.37500	4.21875	3.80208	4.46875
Overall	2.18229	3.69010	3.52604	3.66667	3.92969	4.00521

Table 12. Results of Friedman test over all available satellite images at 2, 3, 4, and 5 levels.

K	Chi-Square Value	p-Value
2	20.1095890410959	$1.19191051533946 \times 10^{-3}$
3	40.6933911159263	$1.08206724960841 \times 10^{-7}$
4	65.6772334293948	$8.10948996472364 \times 10^{-13}$
5	95.8565989847716	$3.94253504591917 \times 10^{-19}$
Overall	194.274459078081	$4.76396506070144 \times 10^{-40}$

3.5.3. Computational Time

Computational time was also one of the important indicators to measure the efficiency of the algorithm. The experimental results at different threshold levels can be found in Table 13 (**bold** is the best). Obviously, the IDSA algorithm is the fastest, although it cannot give the best results in most cases. DHHO/M is a little faster than the traditional HHO, because the greedy selection used in exploitation stage consumes a lot of time; while the dynamic control parameter strategy enables the exploration phase can be adopted in the later iteration, which reduces the complexity to some extent. It is worth noting that evaluating a meta-heuristic algorithm should be comprehensive and objective, not just from a single aspect. The proposed method presents better or at least competitive results in terms of average fitness value, PSNR, MSE, SSIM, and FSIM, despite not the fastest. Thus, DHHO/M can be considered as an efficient technique for multilevel color image segmentation.

Table 13. The average computation time (in seconds) of different algorithms at 2, 3, 4, and 5 levels.

K	DHHO/M	HHO	TLBO	WOA-TH	IDSA	BDE
2	2.198133	2.212233	1.797438	1.844933	1.565033	2.057214
3	2.223321	2.229533	1.800174	1.852567	1.654733	2.151333
4	2.263767	2.339267	1.824733	1.896333	1.663767	2.314633
5	2.342478	2.390067	1.828633	1.927133	1.681547	2.323733

3.5.4. Search Capability on High Dimensional Problems

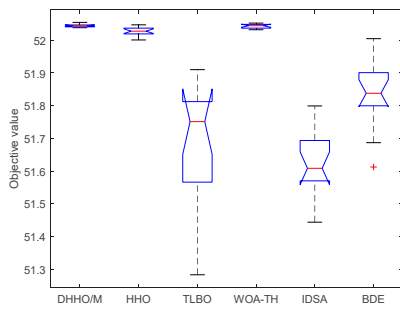
In this section, all available thresholding approaches are compared at K=10, 15, and 20 to assess the performance on high dimensional tasks. Threshold levels selected are the same as [57]. The average fitness function values obtained are presented in Table 14 (**bold** is the best). It can be observed that DHHO/M gives the best results in 22 out of 24 cases (eight images and three thresholds); TLBO and WOA-TH only give the best results in one case respectively, while other algorithms give none. As discussed in above section, the proposed method has shown certain advantages when K = 5, but it is more obvious in higher dimensions. The reason for this phenomenon is that each image can be considered as a different optimization problem, and there is no algorithm can handle all tasks [27]. Even the meta-heuristic algorithm with strong search capability cannot show remarkable performance on all images. Therefore, DHHO/M is more competitive in the field of image segmentation than other algorithms, because it gives the best results in most cases.

Table 14. The fitness values obtained by different algorithms at higher threshold levels.

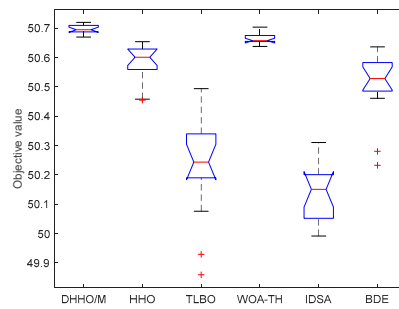
Image	K	DHHO/M	HHO	TLBO	WOA-TH	IDSA	BDE
1	10	34.2109	34.2098	34.2103	34.2107	34.1789	34.1621
	15	43.9417	43.9326	43.9049	43.9337	43.6787	43.8603
	20	52.05	52.0305	51.4385	52.0499	51.6164	51.6291
2	10	33.3497	33.3333	33.3479	33.3494	33.2628	33.333
	15	42.8291	42.8093	42.7608	42.8261	42.6363	42.7508
	20	50.7191	50.5899	50.381	50.67	50.2388	50.3818
3	10	33.8971	33.8945	33.8949	33.8953	33.8526	33.8872
	15	43.7344	43.5907	43.5659	43.735	43.5409	43.6546
	20	51.8463	51.7497	51.2457	51.8042	51.5	51.443
4	10	33.0248	33.0049	32.9986	33.006	32.8715	32.9839
	15	42.5643	42.5557	42.5182	42.5495	42.1679	42.4222
	20	50.404	50.2911	49.8884	50.3453	49.9967	50.2819
5	10	32.1816	32.1393	32.1204	32.1081	32.1083	32.0863
	15	41.5955	41.5162	41.526	41.4936	41.2365	41.315
	20	49.3631	49.1688	48.5774	49.2279	48.3306	49.1217
6	10	33.6055	33.5978	33.5762	33.5641	33.5589	33.5871
	15	43.4567	43.3523	43.2951	43.4393	43.2992	43.4059
	20	51.706	51.6251	51.1347	51.6806	51.2283	51.4454
7	10	32.8232	32.8055	32.825	32.8192	32.6911	32.6068
	15	42.3475	42.3111	42.2273	42.2965	41.9677	42.3149
	20	50.3583	50.2802	49.6741	50.331	49.5638	50.1
8	10	32.8858	32.813	32.8833	32.8505	32.8148	32.825
	15	42.3784	42.2574	42.3384	42.3509	41.9624	42.2916
	20	50.3095	50.2246	50.093	50.2379	49.9046	50.0384

3.5.5. Stability Analysis

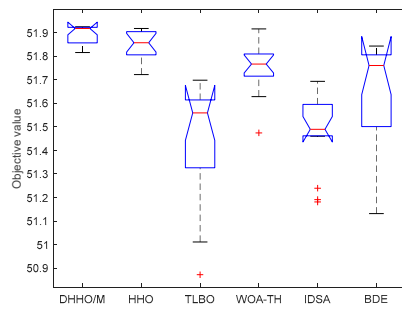
The stability of each algorithm is analyzed and discussed in this section, including two performance measures, namely Std value and boxplot. The Std values obtained on satellite images can be found in Table 7, respectively. A lower Std value indicates better performance. As can be observed, the proposed approach presents the lowest Std values in most cases, showing remarkable stability, continuity and consistency. Furthermore, the boxplot with 20 threshold levels are given in Figure 7, because the difference between the algorithms is more obvious in high dimensions. It can be found that DHHO/M outperforms other approaches again. More specifically, the boxplot obtained is higher in position and more compact, indicating better data consistency. Compared with other algorithms, the proposed method has no bad points (in our study), which illustrates the superiority of DHHO/M based thresholding technique in satellite image segmentation.



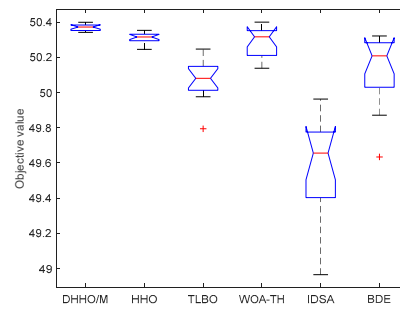
(a) Image1



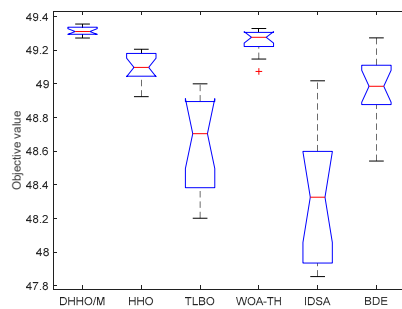
(b) Image2



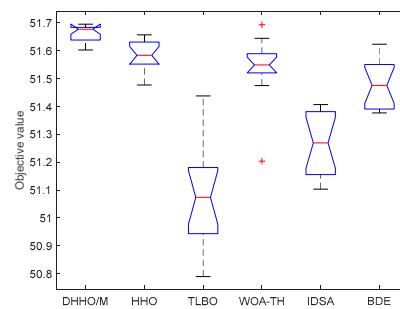
(c) Image3



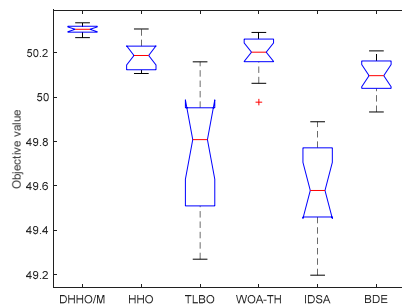
(d) Image4



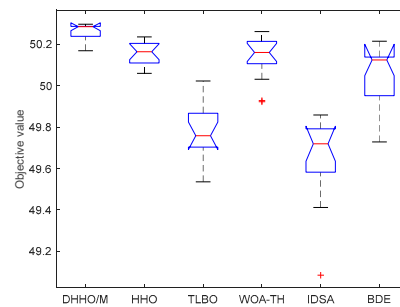
(e) Image5



(f) Image6



(g) Image7



(h) Image8

Figure 7. The boxplot of each method on satellite images (K = 20).

3.5.6. Convergence Property

In this section, the convergence property of DHHO/M algorithm is evaluated. The convergence curves obtained by all algorithms at 20 threshold levels are presented in Figure 8. It is worth mentioning that these figures are drawn in a semi-logarithmic coordinate system for ease of observation. As can be seen, WOA-TH and IDSA are prone to premature convergence and local optimization, which is reflected in the shape of the curve. For example, under the circumstance of “Image3” segmentation, the fitness function values obtained by these two algorithms no longer change after 100 iterations, and obviously they do not get the best value at the end of iteration. Although the fast convergence speed is not a bad characteristic of meta-heuristic algorithm, local optimization seriously affects the accuracy as well as the quality of segmented image. On the contrary, the propose method can better balance the exploration and exploitation stages, neither premature convergence nor slow convergence. Therefore, the DHHO/M based technique can exhibit higher search efficiency in all selected satellite images.

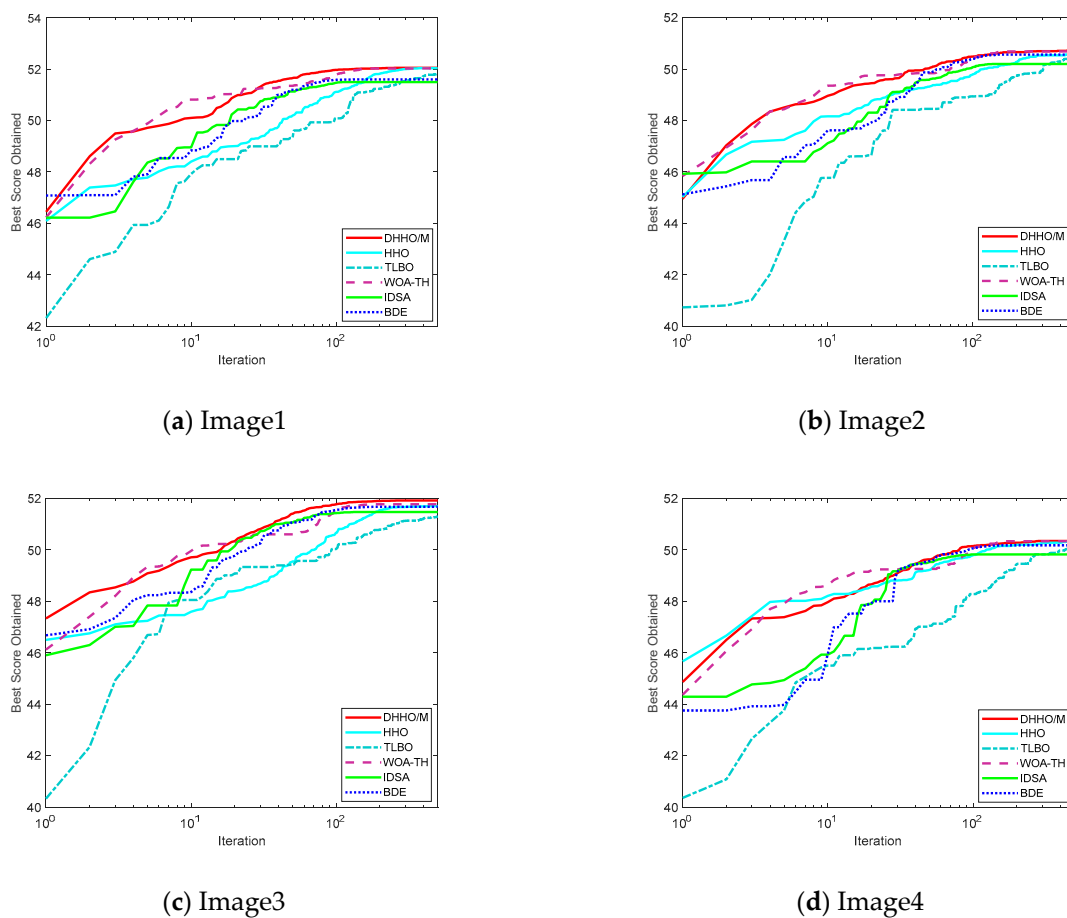
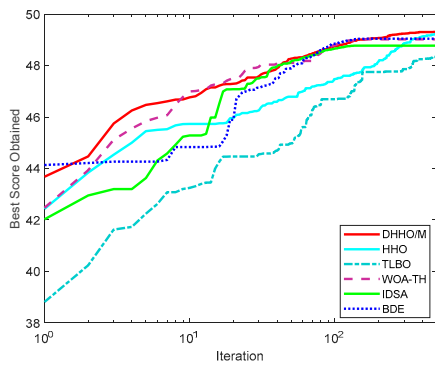
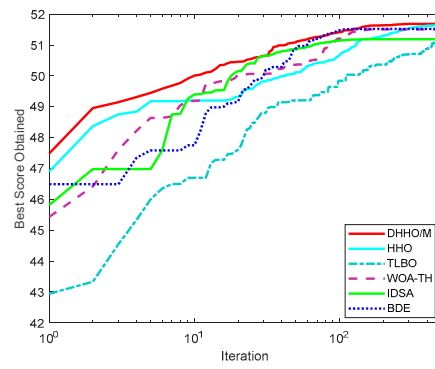


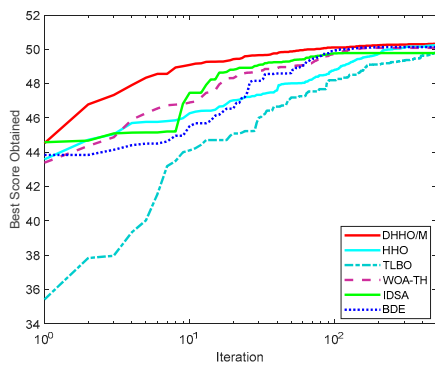
Figure 8. Cont.



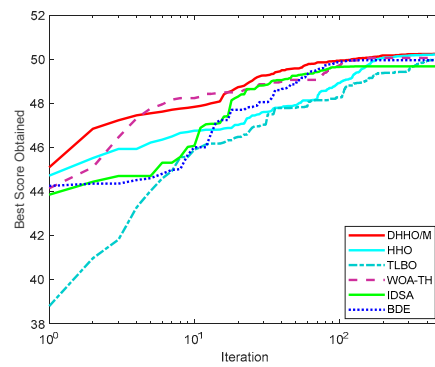
(e) Image5



(f) Image6



(g) Image7



(h) Image8

Figure 8. The convergence curves for fitness function on satellite images (K = 20).

3.6. Experimental Series 4: Performance Using Different Objective Functions

In this section, Tsallis entropy and Otsu between-class variance are served as objective function to assess the feasibility of DHHO/M. Eight different color images are selected from Figure 5. The experiment are conducted on high threshold levels and can be divided into two parts. For the former part, Tsallis entropy based thresholding techniques are selected for comparison, namely the MGOA and MABC. For the latter part, Otsu between-class variance based thresholding approaches are chosen for testing, namely the MFPA and GWO.

The experimental results of Tsallis entropy and Otsu’s method are presented in Tables 15 and 16, respectively (**bold** is the best). As can be observed, DHHO/M gives the best objective function values in all cases, indicating the strong optimization capability. Considering other metrics, the proposed algorithm also produces better or at least competitive results, which shows that the segmented images with more information and details can be obtained. To sum up, the superior performance of the proposed algorithm is not limited to the objective function adopted in this paper, but has potential in other image fields.

Table 15. Comparison of objective value, PSNR, SSIM, and FSIM values based on Tsallis entropy approaches.

Image	K	Objective Value			PSNR		
		DHHO/M	MGOA	MABC	DHHO/M	MGOA	MABC
1	10	3.6662	3.6649	3.6662	30.5093	27.7705	31.1043
	15	5.3316	5.3109	5.3302	34.2626	28.6303	33.4524
	20	6.995	6.948	6.9866	36.8371	33.8588	34.1846
3	10	3.6661	3.665	3.6661	25.7383	24.9989	26.0445
	15	5.3313	5.3141	5.3299	33.3645	28.9334	30.1357
	20	6.9947	6.9516	6.9863	35.3185	32.9205	33.9627
5	10	3.6654	3.6571	3.6654	22.0935	20.8869	21.9164
	15	5.3288	5.3084	5.3262	25.5957	27.7061	27.5186
	20	6.9896	6.837	6.9741	34.1475	33.0881	28.4798
7	10	3.6659	3.6643	3.6658	28.0284	26.1506	27.273
	15	5.3305	5.318	5.3287	33.5291	29.8082	27.8041
	20	6.9924	6.9311	6.9836	36.8653	32.2124	34.0468

Image	K	SSIM			FSIM		
		DHHO/M	MGOA	MABC	DHHO/M	MGOA	MABC
1	10	0.9157	0.8811	0.9225	0.9579	0.9236	0.9622
	15	0.9579	0.8956	0.9495	0.9806	0.9351	0.9762
	20	0.9756	0.9541	0.9638	0.9886	0.9772	0.9773
3	10	0.6904	0.6883	0.6967	0.9156	0.8771	0.9157
	15	0.8827	0.8322	0.8095	0.9636	0.9241	0.9442
	20	0.9251	0.9018	0.8911	0.976	0.9557	0.9633
5	10	0.816	0.7854	0.8113	0.8522	0.8217	0.8501
	15	0.8844	0.8506	0.8368	0.8888	0.8844	0.9139
	20	0.9224	0.9107	0.9077	0.9578	0.9344	0.9298
7	10	0.9001	0.8294	0.8861	0.9376	0.8823	0.9324
	15	0.952	0.9127	0.8916	0.9725	0.939	0.9371
	20	0.9749	0.9468	0.9555	0.9842	0.9549	0.9733

Table 16. Comparison of objective value, PSNR, SSIM, and FSIM values based on Otsu's methods.

Image	K	Objective Value			PSNR		
		DHHO/M	MFPA	GWO	DHHO/M	MFPA	GWO
2	10	1364.9884	1349.264	1363.1902	27.4462	30.0066	27.6228
	15	1376.5148	1365.331	1375.1601	32.3029	33.6342	32.4534
	20	1381.0397	1373.8639	1379.5538	36.5965	35.5419	36.5278
4	10	1304.5892	1289.3595	1304.3497	29.0959	29.2216	29.4061
	15	1315.0389	1302.8059	1314.4674	33.3247	31.413	34.5001
	20	1319.0692	1311.4133	1317.3414	36.1074	36.618	36.1379
6	10	5027.6737	5013.6505	5025.5149	26.5928	23.5726	25.7915
	15	5043.2255	5034.3596	5041.6036	32.9168	27.9594	29.957
	20	5049.6773	5040.9838	5047.5628	35.0998	33.317	33.8307
8	10	934.5128	925.9764	934.3473	31.6049	31.1744	30.8108
	15	943.6876	934.3932	942.2697	35.8537	32.9725	35.0404
	20	947.3744	941.3551	945.2916	37.3744	37.2122	37.3125

Image	K	SSIM			FSIM		
		DHHO/M	MFPA	GWO	DHHO/M	MFPA	GWO
2	10	0.9218	0.8962	0.9106	0.9395	0.9352	0.9337
	15	0.9651	0.9459	0.9577	0.9746	0.9702	0.9688
	20	0.9796	0.9686	0.9779	0.987	0.9824	0.9829
4	10	0.9532	0.9343	0.9487	0.9561	0.9525	0.9533
	15	0.9854	0.954	0.9796	0.9853	0.968	0.979
	20	0.99	0.985	0.9892	0.9899	0.989	0.988
6	10	0.8141	0.7369	0.7833	0.9151	0.8877	0.9125
	15	0.9405	0.8123	0.8654	0.9496	0.9328	0.9619
	20	0.9633	0.9028	0.9269	0.9752	0.9658	0.9723
8	10	0.9271	0.9029	0.9155	0.9571	0.9433	0.9474
	15	0.9655	0.9314	0.9611	0.979	0.9579	0.9798
	20	0.9764	0.9625	0.9745	0.9876	0.9799	0.9856

3.7. Experimental Series 5: Oil Pollution Image Segmentation

In order to further verify the effectiveness of the proposed algorithm in solving practical engineering problems, four oil pollution images are selected for the experiment. These images were taken by the drone in the area of the eighth oil production plant, which can be found in Figure 9 [58]. As can be observed, the oil pollution area of (b) is relatively obvious; while the remaining three images all have strong interference, especially (d). This phenomenon undoubtedly increases the difficulty of segmentation operation, which can be considered as a challenging engineering problem.

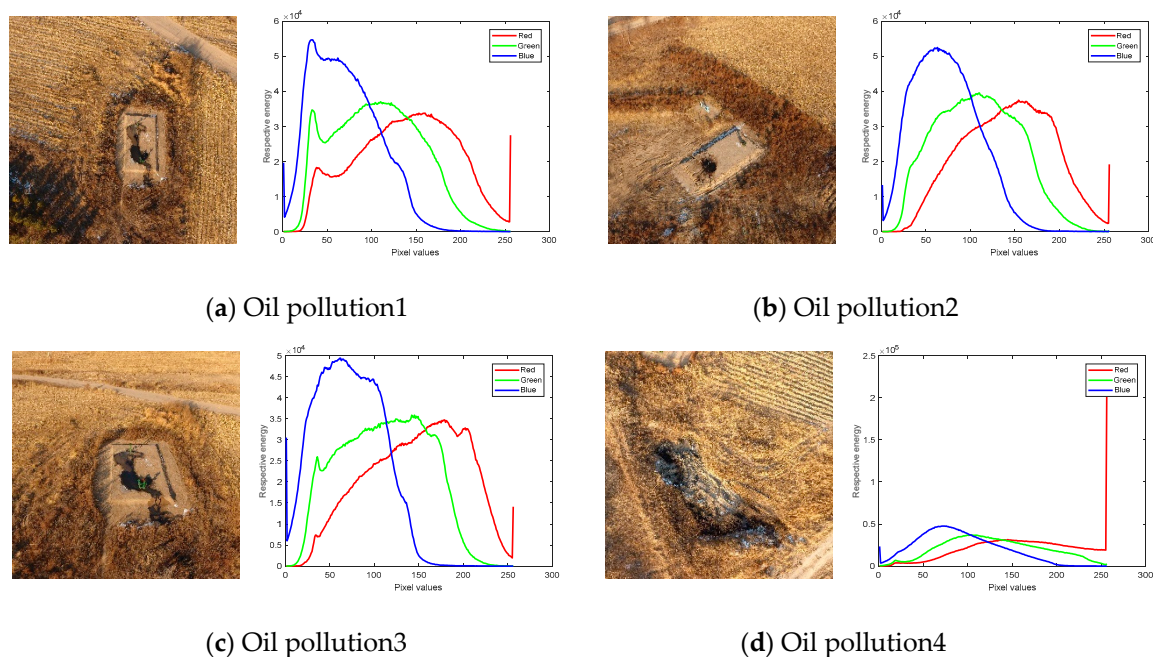


Figure 9. Original oil pollution images and the corresponding histograms for each of color channels (red, green and blue).

The segmented results of the proposed method are presented in Figure 10. Because there is no absolute standard for a real engineering problem, the authors manually labeled the target region and separated it. Then took it as the ground truth for experimental comparison. It can be found from the figures that the oil pollution in (a)–(c) has been successfully separated from the complex background, which is similar to the ground truth. Considering figure (d), the ideal oil pollution area consists of two parts, while the DHHO/M based thresholding technique incorrectly classifies them as a whole. But in fact, it has achieved the desired goal, because the main area of oil pollution has been efficiently identified. To sum up, although the proposed method cannot achieve perfect results for complex images with mixed background and strong interference, it is competent for most cases and can still be considered as a competitive technique for the segmentation of oil pollution image.

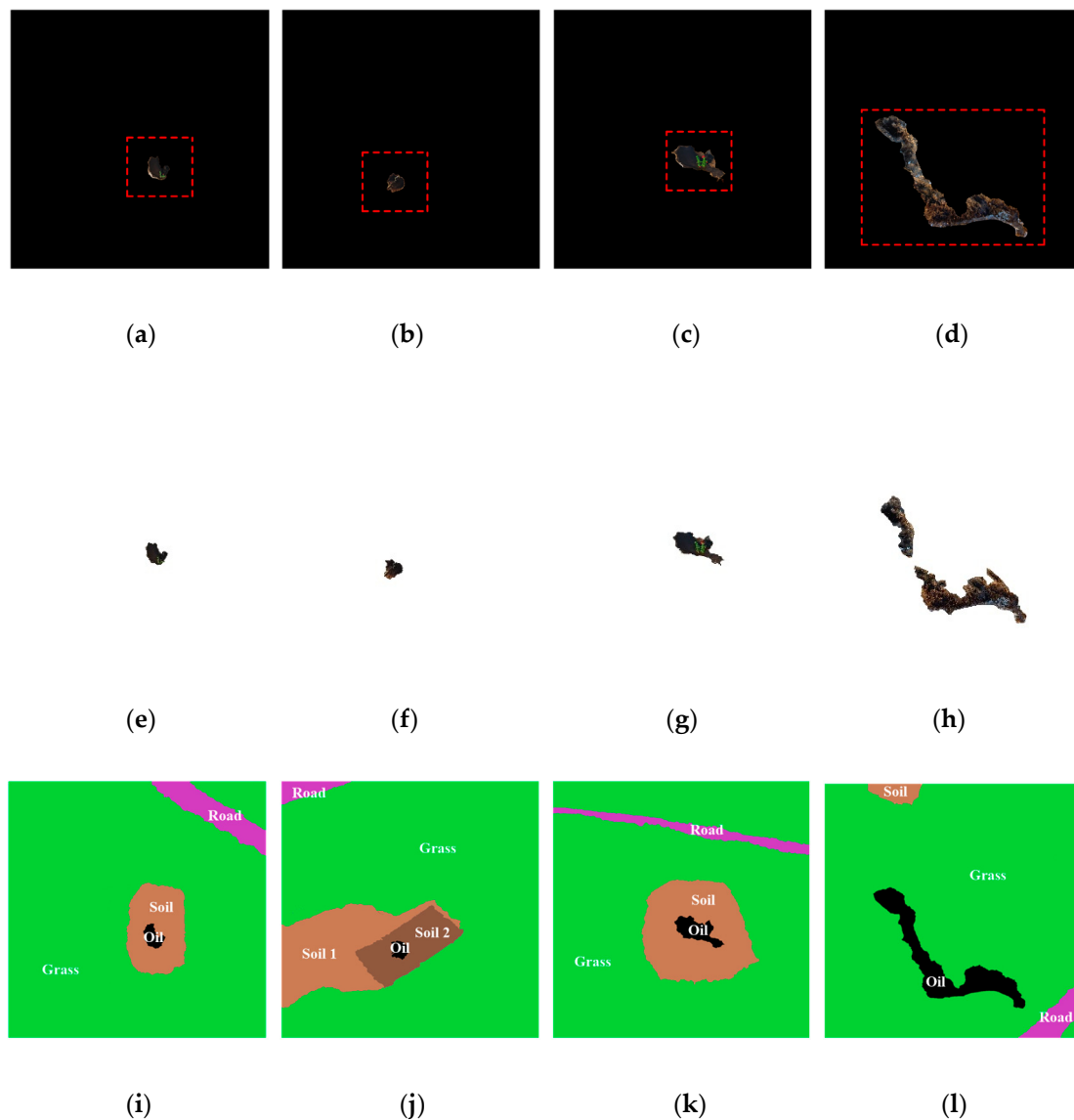


Figure 10. The segmented results and ground truth of the oil pollution images. Panels (a–d) indicate the segmented images, (e–h) show the ground truth, (i–l) indicate the classification result.

4. Conclusions

An efficient satellite image segmentation technique based on DHHO/M is proposed in this paper. Dynamic control parameter strategy and mutation mechanism are used to avoid trapping into the local optimum and improve the search efficiency. In order to validate the superiority of the proposed method, a series of experiments are conducted on various images. For the first part of the experiment, the experimental results indicate that both the improvement strategies adopted can enhance the optimization capability. For the second part of the experiment (the most crucial part), it can be observed that the DHHO/M based technique gives better results for satellite images in terms of objective function value, Std, PSNR, SSIM, FSIM, and convergence property as well as the Wilcoxon's rank sum test and Friedman test. For the third part of the experiment, the robustness of the proposed approach is assessed by the segmentation based on other criteria. For the last part of the experiment, the proposed method is applied to a real engineering problem, namely the segmentation of oil pollution image to further evaluate its practicality and feasibility. The experimental results strongly illustrate the remarkable performance of the DHHO/M based thresholding technique.

In the future, the authors will introduce more efficient technique to handle the images with mixed background and strong interference. Furthermore, due to the conflicts between different criteria, multi-objective optimization for image thresholding is also the research direction.

Author Contributions: H.J. and C.L. contributed to the idea of this paper; C.L. performed the experiments; C.L. wrote the paper; H.J., C.L., D.O., and X.P. contributed to the revision of this paper. W.S. provided fund support.

Funding: This research was supported by the Fundamental Research Funds for the Central Universities (No. 2572019BF04), the National Nature Science Foundation of China (No. 31470714), the Northeast Forestry University Horizontal Project (No. 43217002, No. 43217005, No. 43219002), and the Research Training Project for College Students of Northeast Forestry University.

Acknowledgments: The authors would like to thank the anonymous reviewers for their constructive comments and suggestions.

Conflicts of Interest: The authors declare no conflict of interest.

References

1. Frongillo, M.; Gennarelli, G.; Riccio, G. Plane Wave Diffraction by Arbitrary-Angled Lossless Wedges: High Frequency and Time Domain Solutions. *IEEE Trans. Antennas Propag.* **2018**, *66*, 6646–6653. [[CrossRef](#)]
2. Hinojosa, S.; Avalos, O.; Oliva, D.; Cuevas, E.; Pajares, G.; Zaldivar, D.; Gálvez, J. Unassisted thresholding based on multi-objective evolutionary algorithms. *Knowl. Based Syst.* **2018**, *159*, 221–232. [[CrossRef](#)]
3. Guido, R.C.; Addison, P.; Walker, J. Introducing wavelets and time-frequency analysis. *IEEE Eng. Biol. Med. Mag.* **2009**, *28*, 13. [[CrossRef](#)]
4. Guido, R.C. Practical and useful tips on discrete wavelet transforms. *IEEE Signal Process. Mag.* **2015**, *32*, 162–166. [[CrossRef](#)]
5. Mallat, S.G. A Theory for Multiresolution Signal Decomposition: The Wavelet Representation. *IEEE Trans. Pattern Anal. Mach. Intell.* **1989**, *2*, 674–693. [[CrossRef](#)]
6. Guariglia, E. Entropy and Fractal Antennas. *Entropy* **2016**, *18*, 84. [[CrossRef](#)]
7. Khairuzzaman, A.K.M.; Chaudhury, S. Multilevel thresholding using grey wolf optimizer for image segmentation. *Expert Syst. Appl.* **2017**, *86*, 64–76. [[CrossRef](#)]
8. Hinojosa, S.; Dhal, K.G.; Elaziz, M.A.; Oliva, D.; Cuevas, E. Entropy-based imagery segmentation for breast histology using the Stochastic Fractal Search. *Neurocomputing* **2018**, *321*, 201–215. [[CrossRef](#)]
9. Oliva, D.; Cuevas, E.; Pajares, G.; Zaldivar, D.; Osuna, V. A Multilevel Thresholding algorithm using electromagnetism optimization. *Neurocomputing* **2014**, *139*, 357–381. [[CrossRef](#)]
10. Aziz, M.A.E.; Ewees, A.A.; Hassanien, A.E. Whale Optimization Algorithm and Moth-Flame Optimization for multilevel thresholding image segmentation. *Expert Syst. Appl.* **2017**, *83*, 242–256. [[CrossRef](#)]
11. He, L.; Huang, S. Modified firefly algorithm based multilevel thresholding for color image segmentation. *Neurocomputing* **2017**, *240*, 152–174. [[CrossRef](#)]
12. Díaz-Cortés, M.; Ortega-Sánchez, N.; Hinojosa, S.; Oliva, D.; Cuevas, E.; Rojas, R.; Demin, A. A multi-level thresholding method for breast thermograms analysis using Dragonfly algorithm. *Infrared Phys. Technol.* **2018**, *93*, 346–361. [[CrossRef](#)]
13. Bhandari, A.K.; Kumar, A.; Singh, G.K. Modified artificial bee colony based computationally efficient multilevel thresholding for satellite image segmentation using Kapur's, Otsu and Tsallis functions. *Expert Syst. Appl.* **2015**, *42*, 1573–1601. [[CrossRef](#)]
14. Kapura, J.N.; Sahoob, P.K.; Wongc, A.K.C. A new method for gray-level picture thresholding using the entropy of the histogram. *Comput. Vis. Graph. Image Proc.* **1985**, *29*, 273–285. [[CrossRef](#)]
15. Tsallis, C. Possible generalization of Boltzmann–Gibbs statistics. *J. Stat. Phys.* **1988**, *52*, 479–487. [[CrossRef](#)]
16. Otsu, N. A threshold selection method from gray-level histograms. *IEEE Trans. Syst. Man Cybern.* **1979**, *9*, 62–66. [[CrossRef](#)]
17. Oliva, D.; Hinojosa, S.; Cuevas, E.; Pajares, G.; Avalos, O.; Gálvez, J. Cross entropy based thresholding for magnetic resonance brain images using Crow Search Algorithm. *Expert Syst. Appl.* **2017**, *79*, 164–180. [[CrossRef](#)]
18. Lang, C.; Jia, H. Kapur's Entropy for Color Image Segmentation Based on a Hybrid Whale Optimization Algorithm. *Entropy* **2019**, *21*, 318. [[CrossRef](#)]

19. Jia, H.; Peng, X.; Song, W.; Lang, C.; Xing, Z.; Sun, K. Multiverse Optimization Algorithm Based on Lévy Flight Improvement for Multithreshold Color Image Segmentation. *IEEE Access* **2019**. [[CrossRef](#)]
20. Liang, H.; Jia, H.; Xing, Z.; Ma, J.; Peng, X. Modified Grasshopper Algorithm-Based Multilevel Thresholding for Color Image Segmentation. *IEEE Access* **2019**, *7*, 11258–11295. [[CrossRef](#)]
21. Ouadfel, S.; Taleb-Ahmed, A. Social spiders optimization and flower pollination algorithm for multilevel image thresholding: A performance study. *Expert Syst. Appl.* **2016**, *55*, 566–584. [[CrossRef](#)]
22. Beevi K., S.; Nair, M.S.; Bindu, G.R. Automatic segmentation of cell nuclei using Krill Herd optimization based multi-thresholding and Localized Active Contour Model. *Biocybern. Biomed. Eng.* **2016**, *36*, 584–596. [[CrossRef](#)]
23. Pare, S.; Kumar, A.; Bajaj, V.; Singh, G.K. An efficient method for multilevel color image thresholding using cuckoo search algorithm based on minimum cross entropy. *Appl. Soft Comput.* **2017**, *61*, 570–592. [[CrossRef](#)]
24. Pare, S.; Bhandari, A.K.; Kumar, A.; Singh, G.K. A new technique for multilevel color image thresholding based on modified fuzzy entropy and Lévy flight firefly algorithm. *Comput. Electr. Eng.* **2018**, *70*, 476–495. [[CrossRef](#)]
25. Mlakar, U.; Potočnik, B.; Brest, J. A hybrid differential evolution for optimal multilevel image thresholding. *Expert Syst. Appl.* **2016**, *65*, 221–232. [[CrossRef](#)]
26. Kotte, S.; Pullakura, R.K.; Injeti, S.K. Optimal multilevel thresholding selection for brain MRI image segmentation based on adaptive wind driven optimization. *Measurement* **2018**, *130*, 340–361. [[CrossRef](#)]
27. Wolpert, D.H.; Macready, W.G. No free lunch theorems for optimization. *Evolut. Comput. IEEE Trans.* **1997**, *1*, 67–82. [[CrossRef](#)]
28. Heidari, A.A.; Mirjalili, S.; Faris, H.; Aljarah, I.; Mafarja, M.; Chen, H. Harris hawks optimization: Algorithm and applications. *Future Gener. Comput. Syst.* **2019**, *97*, 849–872. [[CrossRef](#)]
29. Das, S.; Mullick, S.S.; Suganthan, P.N. Recent advances in differential evolution—An updated survey. *Swarm Evol. Comput.* **2016**, *27*, 1–30. [[CrossRef](#)]
30. Bhandari, A.K.; Kumar, A.; Singh, G.K. Tsallis entropy based multilevel thresholding for colored satellite image segmentation using evolutionary algorithms. *Expert Syst. Appl.* **2015**, *42*, 8707–8730. [[CrossRef](#)]
31. Elaziz, M.A.; Oliva, D.; Ewees, A.A.; Xiong, S. Multi-level thresholding-based grey scale image segmentation using multi-objective multi-verse optimizer. *Expert Syst. Appl.* **2019**, *125*, 112–129. [[CrossRef](#)]
32. Agrawal, S.; Panda, R.; Bhuyan, S.; Panigrahi, B.K. Tsallis entropy based optimal multilevel thresholding using cuckoo search algorithm. *Swarm Evol. Comput.* **2013**, *11*, 16–30. [[CrossRef](#)]
33. Xiong, G.; Zhang, J.; Yuan, X.; Shi, D.; He, Y.; Yao, G. Parameter extraction of solar photovoltaic models by means of a hybrid differential evolution with whale optimization algorithm. *Sol. Energy* **2018**, *176*, 742–761. [[CrossRef](#)]
34. Jadon, S.S.; Tiwari, R.; Sharma, H.; Bansal, J.C. Hybrid Artificial Bee Colony algorithm with Differential Evolution. *Appl. Soft Comput.* **2017**, *58*, 11–24. [[CrossRef](#)]
35. Elaziz, M.A.; Xiong, S.; Jayasena, K.P.N.; Li, L. Task scheduling in cloud computing based on hybrid moth search algorithm and differential evolution. *Knowl. Based Syst.* **2019**, *169*, 39–52. [[CrossRef](#)]
36. Xiong, G.; Zhang, J.; Shi, D.; He, Y. Parameter extraction of solar photovoltaic models using an improved whale optimization algorithm. *Energy Convers. Manag.* **2018**, *174*, 388–405. [[CrossRef](#)]
37. Zhao, F.; Xue, F.; Zhang, Y.; Ma, W.; Zhang, C.; Song, H. A hybrid algorithm based on self-adaptive gravitational search algorithm and differential evolution. *Expert Syst. Appl.* **2018**, *113*, 515–530. [[CrossRef](#)]
38. Xu, L.; Jia, H.; Lang, C.; Peng, X.; Sun, K. A Novel Method for Multilevel Color Image Segmentation Based on Dragonfly Algorithm and Differential Evolution. *IEEE Access* **2019**, *7*, 19502–19538. [[CrossRef](#)]
39. Gao, W.; Huang, L.; Wang, J.; Liu, S.; Qin, C. Enhanced artificial bee colony algorithm through differential evolution. *Appl. Soft Comput.* **2016**, *48*, 137–150. [[CrossRef](#)]
40. Ibrahim, R.A.; Elaziz, M.A.; Lu, S. Chaotic opposition-based grey-wolf optimization algorithm based on differential evolution and disruption operator for global optimization. *Expert Syst. Appl.* **2018**, *108*, 1–27. [[CrossRef](#)]
41. Xu, Y.; Chen, H.; Luo, J.; Zhang, Q.; Jiao, S.; Zhang, X. Enhanced Moth-flame optimizer with mutation strategy for global optimization. *Inf. Sci.* **2019**, *492*, 181–203. [[CrossRef](#)]
42. Hijime, K.; Isao, O.; Shingenobu, K. Theoretical Analysis of the Unimodal Normal Distribution Crossover for Real-coded Genetic Algorithms. *Trans. Soc. Instrum. Control Eng.* **2002**, *2*, 187–194.

43. Akimoto, Y.; Nagata, Y.; Sakuma, J.; Ono, I.; Kobayashi, S. Proposal and evaluation of adaptive real-coded crossover AREX. *Trans. Jpn. Soc. Artif. Intell.* **2009**, *24*, 446–458. [CrossRef]
44. Ariyarat, A.; Kanazaki, M. Multi-modal distribution crossover method based on two crossing segments bounded by selected parents applied to multi-objective design optimization. *J. Mech. Sci. Technol.* **2015**, *29*, 1443–1448. [CrossRef]
45. Eshelman, L.J.; Schaffer, J.D. *Real-Coded Genetic Algorithms and Interval-Schemata, Foundations of Genetic Algorithms 2*; Morgan Kaufman Publisher: San Mateo, CA, USA, 1993; pp. 187–202. [CrossRef]
46. Jia, H.; Lang, C.; Oliva, D.; Song, W.; Peng, X. Hybrid Grasshopper Optimization Algorithm and Differential Evolution for Multilevel Satellite Image Segmentation. *Remote Sens.* **2019**, *11*, 1134. [CrossRef]
47. Gill, H.S.; Khehra, B.S.; Singh, A.; Kaur, L. Teaching-learning-based optimization algorithm to minimize cross entropy for Selecting multilevel threshold values. *Egypt. Inf. J.* **2019**, *20*, 11–25. [CrossRef]
48. Bohat, V.K.; Arya, K.V. A new heuristic for multilevel thresholding of images. *Expert Syst. Appl.* **2019**, *117*, 176–203. [CrossRef]
49. Kotte, S.; Kumar, P.R.; Injeti, S.K. An efficient approach for optimal multilevel thresholding selection for gray scale images based on improved differential search algorithm. *Ain Shams Eng. J.* **2018**, *9*, 1043–1067. [CrossRef]
50. Bhandari, A.K. A novel beta differential evolution algorithm-based fast multilevel thresholding for color image segmentation. *Neural Comput. Appl.* **2018**, 1–31. [CrossRef]
51. Landsat Imagery Courtesy of NASA Goddard Space Flight Center and U.S. Geological Survey. Available online: <https://landsat.visibleearth.nasa.gov/index.php?&p=1> (accessed on 7 October 2018).
52. Ewees, A.A.; Elaziz, M.A.; Oliva, D. Image segmentation via multilevel thresholding using hybrid optimization algorithms. *J. Electron. Imaging* **2018**, *27*. [CrossRef]
53. Shen, L.; Fan, C.; Huang, X. Multi-Level Image Thresholding Using Modified Flower Pollination Algorithm. *IEEE Access* **2018**, *6*, 30508–30519. [CrossRef]
54. Frank, W. Individual Comparisons of Grouped Data by Ranking Methods. *J. Econ. Entomol.* **1946**, *39*, 269–270.
55. Friedman, M. The use of ranks to avoid the assumption of normality implicit in the analysis of variance. *J. Am. Stat. Assoc.* **1937**, *32*, 676–701. [CrossRef]
56. Derrac, J.; García, S.; Molina, D.; Herrera, F. A practical tutorial on the use of nonparametric statistical tests as a methodology for comparing evolutionary and swarm intelligence algorithms. *Swarm Evol. Comput.* **2011**, *1*, 3–18. [CrossRef]
57. Mousavirad, S.J.; Ebrahimpour-Komleh, H. Multilevel image thresholding using entropy of histogram and recently developed population-based metaheuristic algorithms. *Evol. Intell.* **2017**, *10*, 45–75. [CrossRef]
58. Jia, H.; Xing, Z.; Song, W. Three Dimensional Pulse Coupled Neural Network Based on Hybrid Optimization Algorithm for Oil Pollution Image Segmentation. *Remote Sens.* **2019**, *11*, 1046. [CrossRef]

